AD-A194 301 EVALUATION OF A DIFFUSION/TRAPPING MODEL FOR HYDROGEN INGRESS IN HIGH-STRENGTH ALLOYS(U) SRI INTERNATIONAL MENLO PARK CA B G POUND 15 APR 88 N00014-86-C-0233 1/1

UNCLASSIFIED F/G 11/6.1 NL

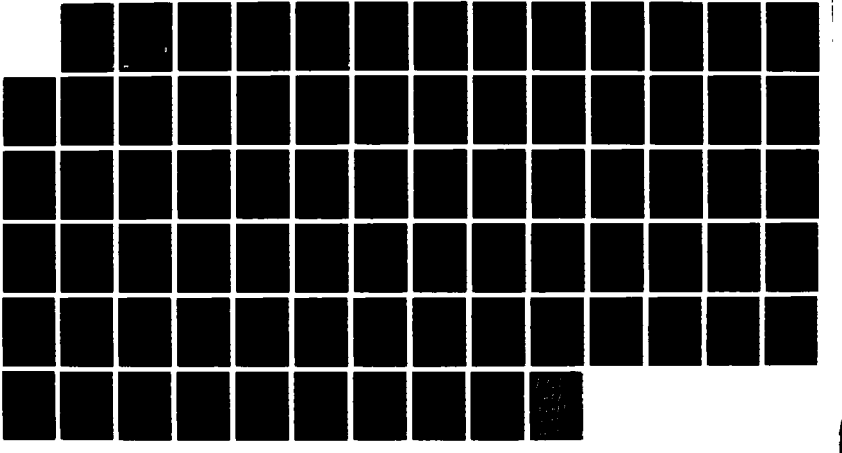

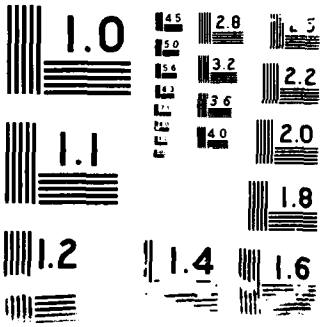
1.0
1.1
1.2
1.4
1.6
1.8
2.0
2.2
2.8
3.2
3.6
4.0
4.5
5.0
5.6

EVALUATION OF A DIFFUSION/TRAPPING MODEL FOR HYDROGEN INGRESS IN HIGH-STRENGTH ALLOYS

April 1988

Final Report

By: Bruce G. Pound
Materials Research Laboratory

Prepared for:

DEPARTMENT OF THE NAVY
Office of Naval Research
800 N. Quincy Street
Arlington, VA 22217

Attention: Dr. A. J. Sedriks

Contract No. N00014-86-C-0233
SRI Project PYU-1962

SRI International
333 Ravenswood Avenue
Menlo Park, California 94025-3493
(415) 326-6200
TWX: 910-373-2046
Telex: 334486

UNCLASSIFIED

SECURITY CLASSIFICATION OF THIS PAGE

REPORT DOCUMENTATION PAGE

1a. REPORT SECURITY CLASSIFICATION Unclassified	1b. RESTRICTIVE MARKINGS
2a. SECURITY CLASSIFICATION AUTHORITY	3. DISTRIBUTION/AVAILABILITY OF REPORT Approved for public release-distribution unlimited. Reproduction in whole or part is permitted for any purpose of the U.S. Gov't.
2b. DECLASSIFICATION/DOWNGRADING SCHEDULE	
4. PERFORMING ORGANIZATION REPORT NUMBER(S)	5. MONITORING ORGANIZATION REPORT NUMBER(S)
6a. NAME OF PERFORMING ORGANIZATION SRI International 6b. OFFICE SYMBOL (If applicable)	7a. NAME OF MONITORING ORGANIZATION
6c. ADDRESS (City, State, and ZIP Code) 333 Ravenswood Avenue Menlo Park, CA 94025-3493	7b. ADDRESS (City, State, and ZIP Code)
8a. NAME OF FUNDING/SPONSORING ORGANIZATION Office of Naval Research 8b. OFFICE SYMBOL (If applicable)	9. PROCUREMENT INSTRUMENT IDENTIFICATION NUMBER N00014-86-C-0233
8c. ADDRESS (City, State, and ZIP Code) Metallic Materials, Code 1131M 800 North Quincy Street Arlington, VA 22217-5000	10. SOURCE OF FUNDING NUMBERS PROGRAM ELEMENT NO. / PROJECT NO / TASK NO / WORK UNIT ACCESSION NO

11. TITLE (Include Security Classification)
Evaluation of a Diffusion/Trapping Model for Hydrogen Ingress in High-Strength Alloys (Unclassified)

12. PERSONAL AUTHOR(S)
B. G. Pound

13a. TYPE OF REPORT	13b. TIME COVERED	14. DATE OF REPORT (Year, Month, Day)	15. PAGE COUNT
Final-Technical	FROM 86Mar15 TO 88Mar15	88 April 15	76

16. SUPPLEMENTARY NOTATION

17. COSATI CODES			18. SUBJECT TERMS (Continue on reverse if necessary and identify by block number)
FIELD	GROUP	SUB-GROUP	4340 Steel, Monel K500, MP35N, hydrogen ingress model hydrogen diffusion, hydrogen trapping, high-strength alloys, hydrogen embrittlement.

19. ABSTRACT (Continue on reverse if necessary and identify by block number)

A diffusion/trapping model for hydrogen ingress was applied to three high-strength alloys, AISI 4340 Steel, Monel K500, and MP35N. The model was used with a potentiostatic double-pulse (PDP) technique, and current transient data were obtained in various electrolytes ranging in pH from 2.9 to 9.0. In all cases, the anodic charge can be analyzed as a function of charging time using an interface control model, in which the rate of hydrogen ingress is determined by the flux across the alloy interface and not by hydrogen diffusion in the alloy. The apparent rate constant for hydrogen trapping (k_a) and the hydrogen ingress flux for each alloy were obtained using this model.

The rate constant for irreversible hydrogen trapping (k) in 4340 steel was evaluated from k_a and was found to be 4 s^{-1}. A simple model of spherical traps was used to calculate the density of irreversible traps from k as 2 x 10^8 m^{-3}. This value is in reasonable agreement with the concentration of MnS inclusions, 2 x 10^9 m^{-3}, but is

20. DISTRIBUTION/AVAILABILITY OF ABSTRACT	21. ABSTRACT SECURITY CLASSIFICATION	
☒ UNCLASSIFIED/UNLIMITED ☐ SAME AS RPT. ☐ DTIC USERS	Unclassified	
22a. NAME OF RESPONSIBLE INDIVIDUAL	22b. TELEPHONE (Include Area Code)	22c. OFFICE SYMBOL

DD FORM 1473, 84 MAR — 83 APR edition may be used until exhausted. All other editions are obsolete.

SECURITY CLASSIFICATION OF THIS PAGE
UNCLASSIFIED

Continuation of Block 19

orders of magnitude smaller than the number of other possible irreversible traps such as Fe_3C and TiC interfaces.

The irreversible trapping constants for Monel K500 and MP35N were also evaluated from k_a, but the densities of irreversible traps were three orders of magnitude smaller than the concentration of sulfur and phosphorus impurities, which were assumed to be the primary irreversible traps. The low values of the trap density are probably primarily due to sulfur and phosphorus segregated as clusters at grain boundaries.

The two nickel-containing alloys, Monel K500 and MP35N, exhibited a lower flux of hydrogen across the alloy surface and a lower irreversible trapping constant than 4340 steel. The difference in both the nature of the principal irreversible traps, which were determined from the trapping constants, and the interfacial flux can be expected to contribute substantially to the difference in susceptibility of the steel and the two nickel-based alloys to hydrogen embrittlement.

Accession For	
NTIS GRA&I	☒
DTIC TAB	☐
Unannounced	☐
Justification	
By	
Distribution/	
Availability Codes	
Dist	Avail and/or Special
A-1	

SUMMARY

Hydrogen ingress in three high-strength alloys, 4340 steel, Monel K500, and MP35N, was shown to occur in all cases under interface control; under the test conditions used, the rate of ingress was controlled by the flux across the alloy surface into the bulk and not by hydrogen diffusion in the alloy. Under interface control conditions, the hydrogen ingress model was valid for a metal independent of the electrolyte used, provided that the electrode surface is unaffected by (1) the electrolyte due to corrosion or a change in any film present, or (2) cathodic charging due to bubble formation or film reduction.

The apparent rate constant (k_a) for hydrogen trapping in 4340 steel was determined for a range of electrolytes, but the values of k_a obtained in all cases except an acetate buffer (pH 4.8) were affected by reactions involving the metal surface itself. The irreversible trapping constant (k) for the steel was therefore obtained from k_a for the acetate and was evaluated by estimating the effect of reversible traps from hydrogen diffusivity data. The value of k for the 4340 steel was 4 s^{-1}, and the density of irreversible traps derived from k, 2 x 10^8 m^{-3}, indicated that the primary irreversible traps were MnS inclusions. The same value of k and therefore trap density was obtained for the steel irrespective of heat-treatment, further indicating that the irreversible traps are stable entities such as MnS inclusions.

The apparent trapping constant for Monel K500 was independent of the electrolyte and was used with diffusivity data to determine the irreversible trapping constant. The value of k was 0.042 s^{-1} which gave a trap density three orders of magnitude less than the trap density expected on the basis of the concentration of sulfur atoms. The value of the calculated trap density was attributed primarily to sulfur segregated as clusters at grain boundaries and secondarily to the effects of the surface film, which may well have a different sulfur concentration than the alloy.

Unlike that for the Monel, the trapping constant measured for MP35N appeared to increase with interfacial pH. This increase is thought to be related to a change in film thickness with increasing pH of electrolyte. Because of a lack of data for the diffusivity of hydrogen in MP35N, the rate constant for irreversible trapping was approximated to the measured value. As for the Monel, the trap density calculated from k was three orders of magnitude less than expected on the basis of the sulfur and phosphorus content in the alloy. This difference was similarly ascribed primarily to sulfur and phosphorus segregated at the grain boundaries and secondarily to effects of the surface film.

The two nickel-containing alloys, Monel K500 and MP35N, exhibit a lower flux of hydrogen across the metal surface and a lower irreversible trapping constant than the steel. The difference in both the nature of the principal irreversible traps, which were determined from the trapping constants, and the interfacial flux can be expected to contribute substantially to the difference in susceptibility of the steel and the two nickel-based alloys to hydrogen embrittlement.

ACKNOWLEDGEMENTS

The author gratefully acknowledges the assistance of Dr. L. Eiselstein of SRI's Poulter Laboratory in providing the 4340 steel plate, heat-treating the 4340 specimens and measuring their hardness.

CONTENTS

FIGURES

TABLES

INTRODUCTION

The ingress of hydrogen into steel and other alloys undergoing corrosion can severely affect the properties of these alloys, especially high-strength steels. In contrast, certain high-strength nickel-based alloys, such as Monel K500 and MP35N, appear to be much more resistant to hydrogen embrittlement, although some failures of these two alloys because of hydrogen embrittlement under severe conditions have been reported.[1,2]

Structural features such as dislocations, internal interfaces, and grain boundaries are potential trapping sites for diffusing hydrogen. The hydrogen atoms are partitioned between the traps and normal lattice sites depending on the energy binding the hydrogen atom to the trapping site, and traps are usually classified as reversible or irreversible. The nature of the traps within a metal critically influences the susceptibility of the metal to hydrogen embrittlement.

A model was developed previously[3] to represent the diffusion and trapping of hydrogen atoms. The model is coupled to the use of a potentiostatic double-pulse (PDP) technique that has been applied[4] to iron in H_2S solutions and was shown to provide quantitative information on both the mobile and trapped hydrogen in the metal. The technique is a transient type rather than one involving steady-state measurements more commonly used for electrochemical studies of hydrogen ingress. Only one other group[5] has reported use of this technique, and their data analysis did not include hydrogen trapping.

In this study, the technique and the associated model were applied to a high-strength steel (AISI 4340) and two high-strength nickel-based alloys (MP35N and Monel K500) to determine the individual hydrogen ingress and trapping characteristics and thereby obtain some insight into the differing resistance of these alloys to hydrogen embrittlement.

THEORY

Previous electrochemical investigations of hydrogen ingress have been concerned mainly with hydrogen diffusion through thin metal membranes using controlled potential or current conditions at both interfaces. In contrast, the PDP technique is applied to sections of bulk metal, typically but not necessarily in rod form. The metal is charged with hydrogen at a constant potential (E_c) for a time (t_c) usually in the range 0.5-40 s. The potential is then stepped to a more positive value, E_A (5-10 mV negative to the open-circuit potential), resulting in an anodic current transient with a charge q_a due to reoxidation of H atoms at the same surface, according to the reaction

$$H_{metal} \text{ ---> } H_{ads} \text{ ---> } H^+ + e^- \qquad (1)$$

where H_{ads} represents hydrogen atoms adsorbed at the metal surface.

The effect of trapping on the diffusion of hydrogen is taken into account by modifying Fick's second law of diffusion. The diffusion/trapping model[3] used with the PDP technique was based on a single trapping term, kc, in which the rate of trapping is assumed to be proportional to the concentration, c(x,t), of diffusing H at point x and time t:

$$dc/dt = D_L(d^2c/dx^2) - kc \qquad (2)$$

where D_L is the lattice diffusivity of hydrogen. In the simplest case, it is assumed that the trapping is entirely irreversible, so there is no significant release of H atoms from the traps. However, equation (2) can be expanded to allow for the effect of reversible traps on the trapping rate constant (k). Iino[6] represented the combination of irreversible and reversible trapping in the diffusion equation as follows:

$$dc/dt + N_i(dn_i/dt) + N_r(dn_r/dt) = D_L(d^2c/dx^2) \quad (3)$$

where

$$(dn_r/dt) = k_r c(1-n_r) - pn_r \quad (4)$$

and

$$(dn_i/dt) = k_i c(1-n_i) \quad (5)$$

The parameters k_r and p are the trapping and release rate constants for reversible traps, N is the density of traps, n is the fraction of traps occupied, and the subscripts i and r refer to irreversible and reversible trapping, respectively. In his treatment, Iino assumed a low trap coverage in both the irreversible and reversible cases, so $n_i \ll 1$ and $n_r \ll 1$. Therefore, equation (4) reduces to $(dn_r/dt) = k_r c - pn_r$ and equation (5) to $(dn_i/dt) = k_i c$.

It is further assumed[7] that there is local equilibrium between the trapped hydrogen and the lattice hydrogen at the reversible sites; that is, $(dn_r/dt) = 0$ for a given value of c. Therefore, $n_r = k_r c/p$, and because $c = f(t)$, the rate of reversible trapping is given by

$$(dn_r/dt) = k_r/p(dc/dt) \quad (6)$$

The diffusion equation (3) can then be expressed as

$$dc/dt + N_i k_i c + (dc/dt)N_r k_r/p = D_L(d^2c/dx^2) \quad (7)$$

and therefore

$$(dc/dt)(1 + N_r k_r/p) + N_i k_i c = D_L(d^2c/dx^2) \quad (8)$$

McNabb and Foster[8] derived an apparent diffusion coefficient given by $D_L/(1 + N_r k_r/p)$, and it is evident that division of equation (8) by $(1 + N_r k_r/p)$ will similarly give an apparent diffusion coefficient, D_a, and also yield an apparent or measured trapping constant, k_a:

$$dc/dt + N_i k_i c/(1 + N_r k_r/p) = [D_L/(1 + N_r k_r/p)](d^2c/dx^2) \quad (9)$$

$$dc/dt + k_a c = D_a(d^2c/dx^2) \quad (10)$$

where $k_a = k/(1 + K_r)$ and $D_a = D_L/(1 + K_r)$. The irreversible trapping constant, k, is given by $N_i k_i$, and K_r is an equilibrium constant defined as $N_r k_r/p$. Equation (10) has also been derived elsewhere by a similar treatment.[9]

The effect of reversible traps on k can therefore be taken into account through the equilibrium constant for reversible traps. Because the equilibrium constant also relates the apparent diffusivity to the lattice diffusivity, the value of K_r can be determined from diffusivity data if such data are available for the alloy of interest and for the lattice of the primary components of the alloy.

On the basis of the relatively short charging times (≤40 s) used in the PDP technique, the irreversible traps are believed not to become saturated; that is, the experimentally-determined irreversible trapping constant, k, does not vary with charging time. The expression for the rate of trapping postulated by McNabb and Foster,[8] $k'N(1 - n)c$, is consistent with equation (2) if it is assumed that $(1 - n)$ is constant on the time scale of the potential-step experiments. The irreversible trapping constant is then given by $k = k'N(1 - n)$, which, for low trap coverage, corresponds to the expression $N_i k_i$ given above.

Furthermore, the reversible traps are assumed to release all their hydrogen during the anodic transient, t_a, so that all the hydrogen remaining

in the metal at the end of t_a is truly irreversibly trapped. In the case of 4340 steel, the assumption of highly reversible traps is based on a value of 500 estimated for K_r (see below). The density of reversible traps in 4340 steel[10] is typically in the range 10^{19}-10^{27} m^{-3}. Even at the lower limit of this range, $k_r/p = 5 \times 10^{-17}$ m^3, which implies that the release constant is large, and so the release rate will be high even when the fraction of traps occupied is very low. In the case of the two nickel-based alloys, the binding energy for hydrogen to defects such as vacancies or edge dislocations in an fcc lattice is about 0.1 eV; in comparison, the activation energy for diffusion in this type of lattice is roughly 0.4 eV.[11] Therefore, transport of hydrogen in these alloys is limited by diffusion, with little hindrance from reversible traps.

The form of equation (10) is identical to that of equation (2), which has been solved analytically[3] for two cases characterized by the rate-determining step for the transfer of H_{ads} into the metal during the charging time. In both cases, it is assumed that that the layer of H_{ads} adjusts very rapidly to a potential step. For a given value of the charging potential, E_c, the hydrogen ingress flux into the metal is considered constant. If equilibrium is established between the concentration of hydrogen in the metal at $x = 0$ and the adsorbed hydrogen layer, the ingress of hydrogen will be controlled by diffusion in the bulk metal. However, if the flux across the interface is very slow, the rate of ingress will be determined by the flux. In this case, hydrogen ingress occurs under interface control.

EXPERIMENTAL PROCEDURE

Materials

The chemical composition of each alloy was provided by the manufacturer and is given in Table 1.

Table 1

CHEMICAL COMPOSITION OF THE THREE ALLOYS TESTED (wt%)*

Element	4340 steel	Monel K500	MP35N
Fe	Bal	0.64	0.34
C	0.42	0.16	0.003
Mn	0.46	0.72	<0.01
P	0.009	n	0.003
S	0.001	0.001	0.002
Si	0.28	0.15	0.02
Cu	0.19	29.99	n
Ni	1.74	64.96	35.88
Cr	0.89	n	20.19
Mo	0.21	n	9.55
Al	0.031	2.92	n
N	0.005	n	n
O	0.001	n	n
Ti	n	0.46	0.85
Co	n	n	Bal

* Bal = balance, n = not present or not given.

The 4340 steel was supplied as 1.27-cm plate produced from an argon-oxygen-decarburized heat and subsequently vacuum-arc remelted (VAR) before being forged, rolled, and annealed. The as-received plate was machined

into two rods 1.25 cm in diameter and 5 cm long, which were heat treated to Rockwell C hardness (HRC) values of 41 and 53. These values correspond to yield strengths of 175 and 260 ksi, respectively. The conditions of heat treatment are shown in Table 2.

Table 2

CONDITIONS OF HEAT TREATMENT FOR 4340 STEEL

Step	HRC 41	HRC 53
Austenized	830°C for 45 min	850°C for 45 min
Quench	Oil	Oil
Tempered	450°C for 60 min	180°C for 80 min
Quench	Water	Water

MnS inclusions are well-recognized as strong hydrogen traps,[12-15] and a thermal analysis study[15] of 4340 steel showed that the temperature for hydrogen release increases in the following order: ferrite-carbide interface < dislocation < microvoid < MnS interface. Accordingly, MnS inclusions are likely to be principal irreversible trapping sites in 4340 steel. In an earlier study in which the nature and distribution of inclusions in the 4340 steel used in this work were determined,[16] it was found that there were $\sim 10^5$ m^{-2} MnS inclusions randomly distributed through the material. The inclusions were ellipsoidal with the major axis transverse to the rolling direction. On the basis that the inclusions were spherical, the concentration of inclusions was calculated to be 2×10^9 m^{-3} and the mean radius of the inclusions averaged over the transverse and parallel directions was 9.2 μm.

The Monel K500 was supplied by Huntington Alloys as an unaged, 1.27-cm,

cold-drawn rod. The HRC value of the as-received (AR) material was 26, which corresponds to a yield strength of ~110 ksi. A section of the rod was age-hardened to HRC 35, giving a yield strength of about 159 ksi. The age-hardening was performed according to the procedure recommended by the manufacturer: Heat for 8 h at 600°C and then cool to 480°C at a rate of 11°/h.

MP35N is based on the quaternary of cobalt, nickel, chromium, and molybdenum. It is a vacuum-induction, vacuum-arc remelted alloy and was supplied by Latrobe Steel Co. as a 1.36-cm cold-drawn rod that had been aged by heating at 590°C for 4 h and then air-cooling. The hardness and yield strength for the as-received material were HRC 45 and 269 ksi, respectively.

Electrodes

The test electrodes of each alloy were fabricated from 5-cm lengths of rod. A stainless steel rod 3 mm in diameter screwed into one end of the rods to support the electrode in the cell and provide electrical contact. Each rod was press-fitted into a Teflon sheath so that only the planar end surface of the rod was exposed to the electrolyte. The surface was polished with successively finer grades of SiC paper from 320 to 600 grit followed by 0.05-μm alumina powder.

Cell

A conventional three-electrode electrochemical cell was used. The counter electrode was a graphite rod, and the reference electrode assembly consisted of a saturated calomel electrode (SCE) inserted in a Luggin probe. All potentials are given with respect to the SCE. Various electrolytes ranging in pH from 2.9 to 9.0 (Table 3) were used.

Table 3

COMPOSITION AND pH OF TEST ELECTROLYTES

Designation	Composition	pH*
Sulfuric acid	0.0009 mol L^{-1} H_2SO_4	2.9
Acidified chloride	3 wt% NaCl 3.7×10^{-5} mol L^{-1} HCl	4.5
Acetate buffer	1 mol L^{-1} CH_3COOH 1 mol L^{-1} CH_3COONa	4.8
Phosphate buffer	0.5 mol L^{-1} Na_2HPO_4 0.5 mol L^{-1} NaH_2PO_4	6.7
Bicarbonate buffer	0.5 mol L^{-1} $NaHCO_3$ 0.01 mol L^{-1} NaOH	9.0

* Measured values

Each electrolyte contained 15 ppm As_2O_3 as a hydrogen entry promoter. The electrolyte was deaerated with argon for 1 hour before measurements began and throughout data acquisition. All measurements were performed at 22 ± 2°C.

Instrumentation

The PDP technique was performed using a Princeton Applied Research Model 173 potentiostat with a Model 276 interface coupled to a Macintosh microcomputer via an Iotech Mac 488A bus controller. A BASIC program, PDP 173/488 (Appendix A), was developed to provide the perturbation (double-pulse) waveform, set control parameters, and acquire current data. The open-circuit potential (E_{oc}) of the test electrode was sampled before each

charging time (t_c) and the electrode was then potentiostatically controlled at E_A, which was set to 10 mV negative of E_{oc}. This approach allows for any drift in E_{oc} and therefore reflects the corrosion state of the metal at all times during the range of E_c and t_c values used. The practical consequence of this procedure is that E_A is always maintained slightly negative of the existing E_{oc}, and thus anodic oxidation of the metal is minimized.

Control Parameters

The principal control parameters are the charging potential (E_c), the period of the anodic and cathodic transients (t_a and t_c, respectively), and the current sampling rate. These parameters have several electrochemical and metallurgical limitations.

The primary concern is to generate a sufficiently rapid discharge of H^+ during t_c to transfer a significant quantity of hydrogen into the metal. However, it is undesirable for molecular hydrogen to form to an extent that an appreciable number of bubbles develop on the surface, because the bubbles would influence the surface coverage of H_{ads} and also reduce access of the electrolyte to the surface. These factors are determined by the hydrogen evolution kinetics of the alloy, and consequently the magnitude of the cathodic potential step was varied according to the alloy being tested.

The cathodic charging times were selected to vary from 0.5 to 40 s, which provided a range covering almost two decades. With charging times under 0.5 s, insufficient hydrogen enters the metal, and with very short charging times, the current is dominated by charging of the double layer at the surface. With prolonged charging of the metal, irreversible traps may become saturated, and the mathematical model used in the analysis would be invalidated. Moreover, excessively long charging times might cause internal damage to the metal due to the accumulation of hydrogen. The reproducibility of anodic charge data in consecutive tests with t_c = 40 s suggested that traps were neither saturated nor generated as a result of structural damage.

The time of data acquisition (t_a) during the anodic transient was made equal to that for the cathodic transient on the basis that this time would be long enough for the deepest untrapped hydrogen to diffuse back to the metal surface and for hydrogen in highly reversible traps to be released, as discussed above. Accordingly, it was assumed that q_a is equal to the anodic charge $q'(\infty)$ corresponding to $t_a = \infty$ (see below).

The sampling time for the current was usually selected to allow sufficient resolution of the current transient. Various sampling times were tested. Table 4 shows the values selected and the total number of data points acquired during the anodic and cathodic transients for each charging time; the anodic and cathodic parts each contain half the number of points shown.

Table 4

DATA ACQUISITION CHARACTERISTICS

t_c (s)*	Sampling time (ms)	Number of points
0.5	5	200
1	5	400
2	5	800
5	10	1000
10	20	1000
15	30	1000
20	40	1000
25	50	1000
30	50	1200
40	50	1600

* $t_a = t_c$

RESULTS

Method of Analysis

The anodic current transients for all three alloys characteristically exhibited the same shape over the range of charging potentials and times of interest. A typical current/time (i/t) transient is shown in Fig. 1. In all cases, analysis of the data in terms of the diffusion-control model indicated that (1) k_a varied according to the number of points analyzed from the transient for each value of t_c, (2) k_a decreased with increasing t_c for a given potential, and (3) k_a generally decreased with an increase of potential for a given t_c. The diffusion control model therefore was not valid for any of the three alloys, but in all cases the data could be analyzed in terms of the interface control model. According to the interface control model, the total charge passed out is given in nondimensional form by[3]

$$Q'(\infty) = \sqrt{R}\{1 - e^{-R}/\sqrt{(\pi R)} - [1 - 1/(2R)]\mathrm{erf}\sqrt{R}\} \quad (11)$$

The nondimensional terms are defined by $Q'(\infty) = q'(\infty)/[FJ\sqrt{(t_c/k_a)}]$ and $R = k_a t_c$ where J is the ingress flux in mol cm^{-2} s^{-1} and the anodic charge $q'(\infty)$ is equated to q_a in mC cm^{-2}. For the model to be applicable, it must be possible to determine a trapping constant for which the ingress flux is constant over the range of charging times. The data were analyzed using the BASIC program, INTERFACE, given in Appendix B. The values for the trapping constant and flux can be used to calculate the amount of charge (q_T) irreversibly trapped under conditions of interface control for which the trapped charge is given nondimensionally by

$$Q_T = [\sqrt{R} - 1/(2\sqrt{R})]\mathrm{erf}\sqrt{R} + e^{-R}/\sqrt{\pi} \quad (12)$$

The data analysis using the interface control model was restricted to charging times of 10 to 40 s. There are two reasons for this restriction: (1) At short charging times, the values of q_a may include a significant

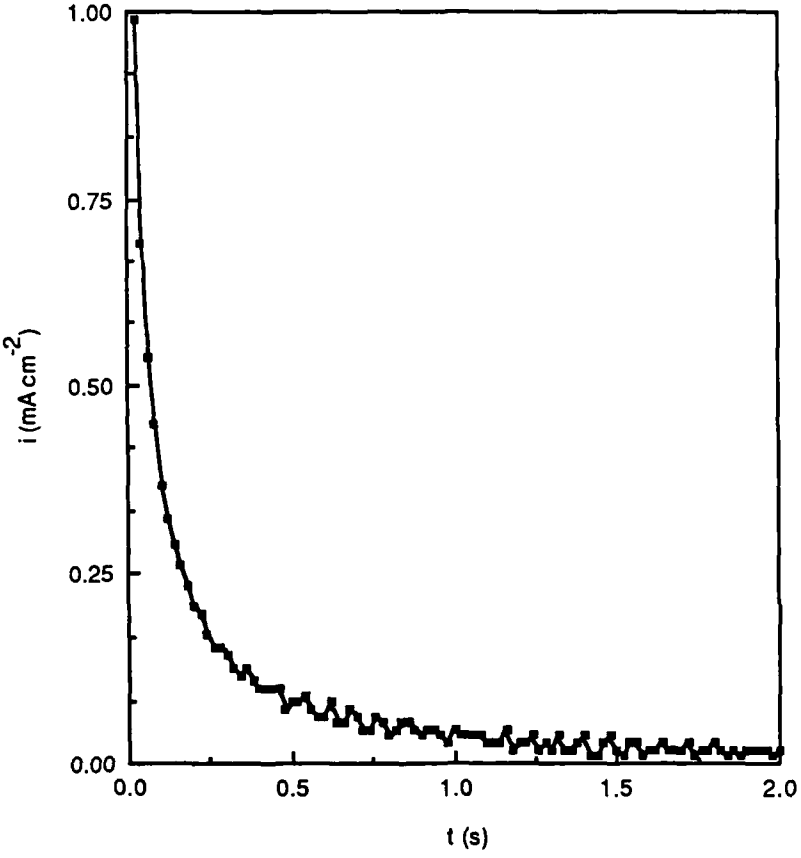

Figure 1. Anodic transient for 4340 steel HRC 53 in acetate buffer.
t_c = 10 s; E_c = -0.985 V (SCE)

The full transient is not shown.

contribution due to oxidation of the adsorbed hydrogen layer, q_{ads}, and the model assumes that q_a is associated entirely with oxidation of hydrogen that entered the metal. (2) The cathodic current during t_c changes to some extent in its early stages, and this change may affect the flux of hydrogen across the metal surface. The model assumes that mass transport of H^+ to the metal surface during t_c is constant, and this assumption is more justified for values of $t_c \geq 10$ s, where the current is approximately constant for most of the charging time.

4340 Steel

The anodic charge as a function of t_c could generally be analyzed with the interface control model to the extent that values of the apparent trapping constant and flux were obtainable. However, the steel was susceptible to film formation or metal dissolution in all the electrolytes except the acetate buffer. In such cases, the validity of the results was uncertain because anodic reactions involving the alloy itself appeared to introduce significant errors into the values of q_a for H atom oxidation, and thereby cause anomalies in the results for k_a and J.

Consistent values were obtained with the acetate buffer, which proved to be the most suitable electrolyte for this type of study because it provided an adequate and steady supply of H^+ for reduction but was not so acidic as to cause substantial attack of the alloy. Accordingly, the results for this electrolyte are presented first for all three alloys tested.

Acetate. Values of q_a were plotted against $\sqrt{t_c}$, which was used to be consistent with the previous work,[3,4] and data for a potential step, η ($E_c - E_{oc}$), of -0.4 V [E_c = -0.985 V (SCE)] are shown in Fig. 2. The anodic charge (q_{ads}) arising from oxidation of the adsorbed H layer can be estimated by extrapolation to $t_c = 0$, and therefore, data are displayed only for shorter charging times ($t \leq 15$ s) to show the extrapolated curve more clearly; the full range of data is presented in Fig. 3.

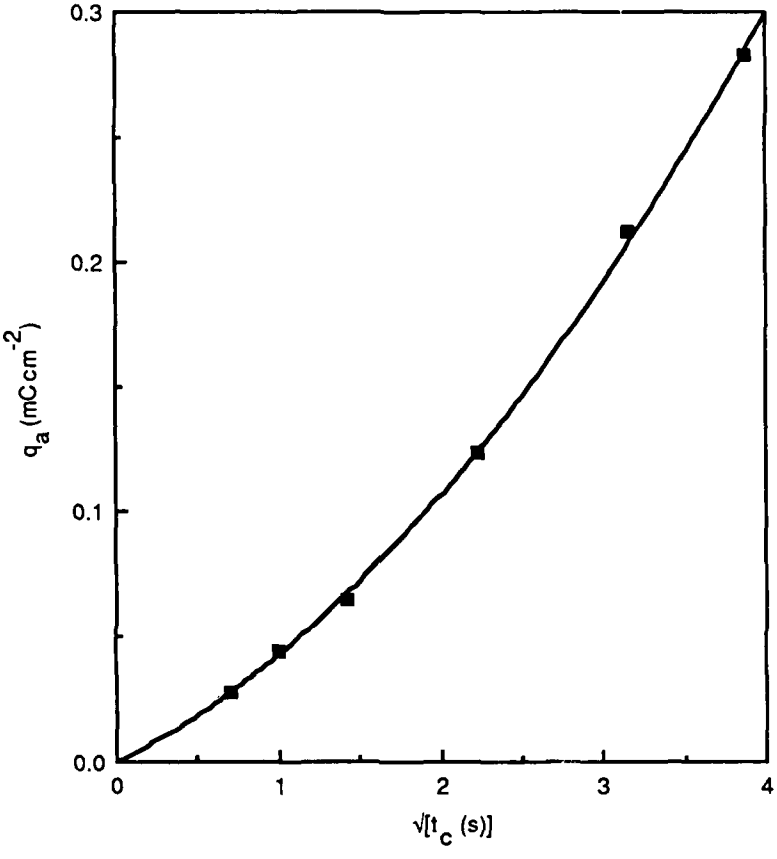

Figure 2. Dependence of anodic charge on charging time for 4340 steel HRC 53 in acetate buffer.

t_c = 10 s; E_c = -0.985 V(SCE)

The dependence of q_a on t_c can be represented by a second-order polynomial:

$$q_a = 7.9 \times 10^{-5} + 0.031\ t_c^{1/2} + 0.011\ t_c \qquad (13)$$

whereas in the absence of trapping, q_a is expected to vary linearly with t_c.[3] From equation (13), it is apparent that $q_{ads} < 10^{-4}$ mC cm^{-2} which can be regarded as negligible. Accordingly, q_a is assumed to be associated entirely with absorbed hydrogen.

The data for both heat-treated specimens were analyzed using the interface control model. Values of the interfacial flux and apparent trapping constant determined for charging times from 10 to 40 s are given for each potential step in Table 5. In both cases, current transients were obtained at a lower overpotential (-0.25 V), but the results for q_a were too low to determine reliable values for k and J.

Table 5

INTERFACIAL FLUX AND TRAPPING CONSTANTS FOR 4340 STEEL IN ACETATE

Type	η (V)	J (nmol cm^{-2} s^{-1})	k_a (s^{-1})
HRC 41	-0.30	0.045	0.009
	-0.35	0.07	0.006
	-0.40	0.19	0.008
	-0.45	0.36	0.008
HRC 53	-0.30	0.07	0.008
	-0.35	0.13	0.007
	-0.40	0.26	0.008
	-0.45	0.55	0.009

For both heat-treated specimens, k_a is essentially independent of η, as expected, because the density of traps within the metal should not be affected by the electrochemical surface conditions. Moreover, in both cases k_a has approximately the value 0.008 s^{-1}. Using this value for k_a and the appropriate value of J in equation (11), q_a was calculated for charging times from 0.5 to 40 s and compared with the corresponding experimental results. The two sets of data for the HRC 53 steel charged at η = -0.4 V are shown in Fig. 3, where Q' is given by $Q'(\infty)\sqrt{(t_c/k)} = q_a/FJ$. The form of the curves and the close fit between them are typical for both specimens. The agreement between the two sets of data indicates the independence of both k and J with respect to t_c.

In contrast, the flux does increase with η as a result of the dependence of J on the surface coverage of H_{ads} and therefore on potential. The surface coverage and hence the flux should exhibit an exponential dependence on potential, which is in fact observed for both specimens, as shown in logarithmic form in Fig. 4. The regression coefficients (r) are 0.99 and 1.00, and interestingly, although the amount of data is limited, the two slopes (m = -6.29 and -5.97) appear to be close. This closeness suggests that the rate constant for the flux across the interface is determined primarily by electrochemical characteristics and not by alloy microstructure.

The dimensionalized trapped charge (q_T) for 4340 steel was calculated using equation (12). The data for the HRC 53 specimen charged at η = -0.4 V are given in Table 6, which also shows the experimental data for the anodic charge (q_a) and cathodic charge (q_c) passed during the respective potential pulses and the charge associated with the entry of hydrogen into the metal (q_{in}) given by the sum of q_T and q_a. The cathodic charge was shown to be linearly dependent on t_c (Fig. 5). This linear dependence indicates that the cathodic current, and therefore supply of H^+, was essentially constant even for relatively low charging times. The data for q_{in}, q_T, and q_c were used to obtain two ratios: (1) q_T/q_{in}, corresponding to the fraction of hydrogen in the metal that was trapped; and (2) q_{in}/q_c, representing the fraction of

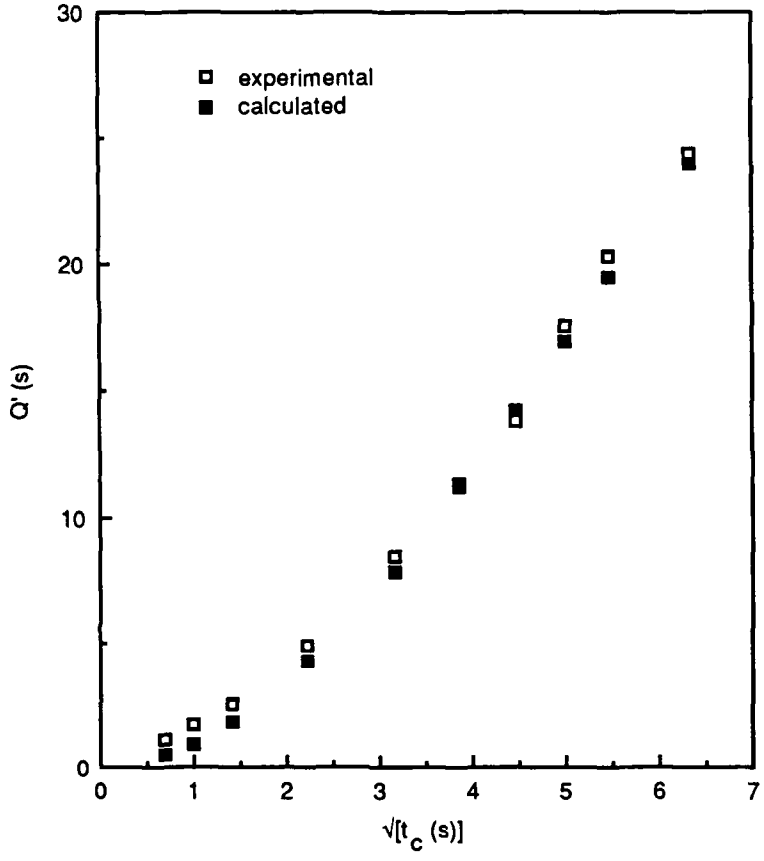

Figure 3. Comparison of anodic charge data for 4340 steel HRC 53 in acetate buffer.

E_c = -0.985 V(SCE)

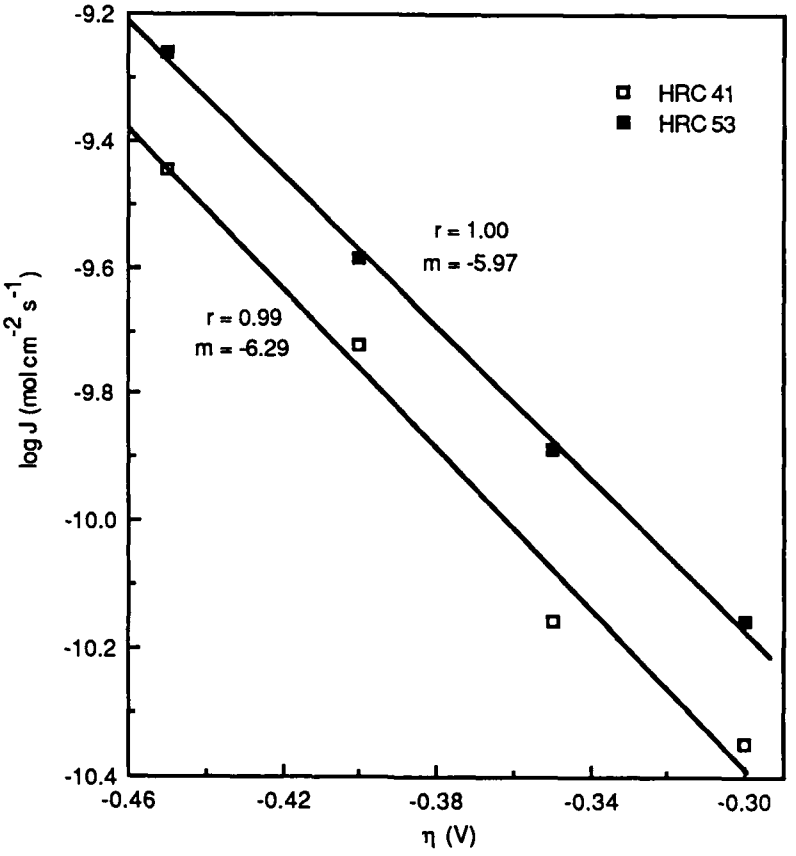

Figure 4. Dependence of flux on overpotential for 4340 steel in acetate buffer.

charge associated with hydrogen entry during the charging step.

Table 6

CHARGE PARAMETERS[a] FOR 4340 STEEL HRC 53 IN ACETATE[b]

t_c (s)	q_T	q_a	q_{in}	q_T/q_{in}	q_c	$\lvert q_{in}/q_c \rvert$
0.5	0.001	0.028	0.029	0.021	-0.62	0.046
1	0.002	0.044	0.046	0.037	-1.23	0.037
2	0.005	0.064	0.069	0.069	-2.37	0.029
5	0.019	0.123	0.142	0.132	-5.67	0.025
10	0.053	0.212	0.265	0.199	-10.96	0.024
15	0.096	0.283	0.379	0.253	-16.67	0.023
20	0.146	0.345	0.491	0.298	-22.74	0.022
25	0.203	0.441	0.644	0.315	-29.03	0.022
30	0.265	0.560	0.825	0.321	-35.28	0.023
40	0.401	0.611	1.012	0.397	-47.55	0.021

[a] The units of charge are mC/cm^2.

[b] η = -0.4 V; used $k_a = 0.008\ s^{-1}$, $J = 0.26$ nmol $cm^{-2}\ s^{-1}$ for q_T.

The ratio q_T/q_{in} has a small potential dependence and increases with t_c from about 1-2 to 35-42% over the range 0.5-40 s for η = -0.35 to -0.45 V. This increase shows that the proportion of hydrogen being trapped increases with the amount of hydrogen entering the alloy because of differences in the dependence of q_T and q_{in} on t_c; q_{in} varies linearly[3] with t_c, whereas the relationship between q_T and t_c is more complex [see equation (12)]. The dependence of q_{in} on t_c for the HRC 53 specimen (η = -0.4 V) is shown in Fig. 6. As expected, a linear relationship is obtained with a slope of $FJ = 25.3\ \mu C\ cm^{-2}\ s^{-1}$, corresponding to the same value of the flux (0.26 nmol $cm^{-2}\ s^{-1}$) used in equation (12).

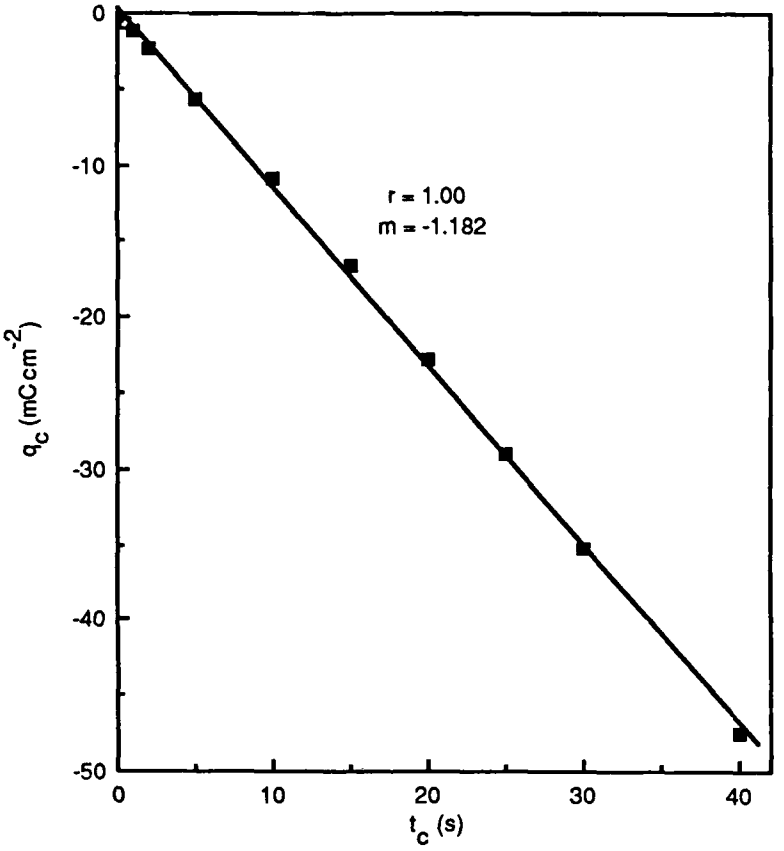

Figure 5. Dependence of cathodic charge on charging time for 4340 steel HRC 53 in acetate buffer.

E_c = -0.985 V(SCE)

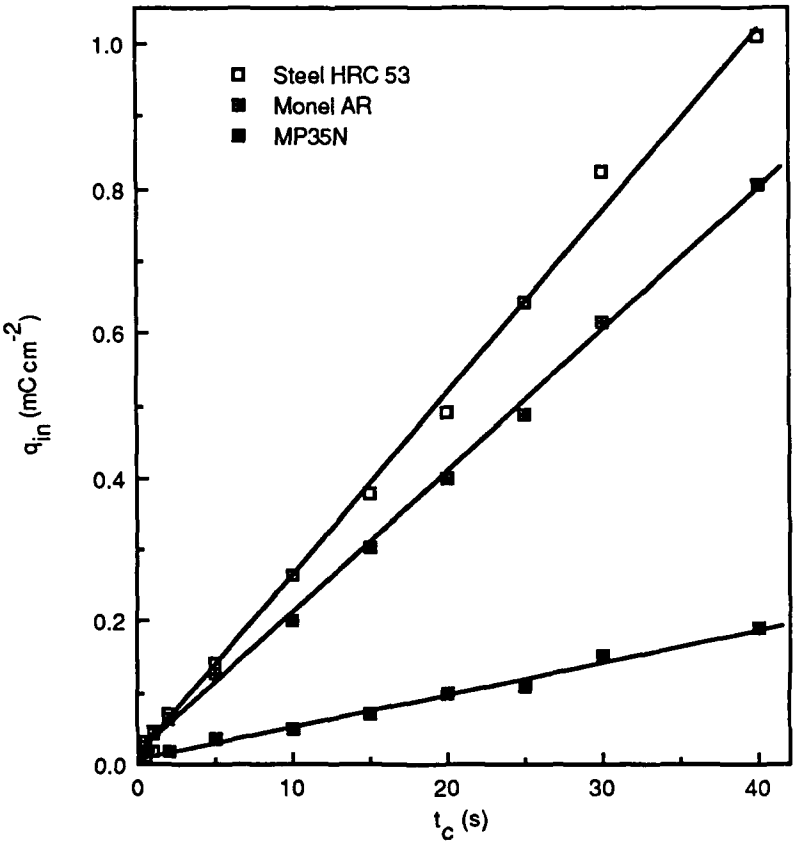

Figure 6. Dependence of ingress charge on charging time for 4340 steel HRC 53, Monel K500 AR, and MP35N in acetate buffer.

E_c (SCE) = -0.985 V for steel; -0.905 V for Monel; -0.425 V for MP35N

Despite the complex variation of q_T with t_c, q_T/q_{in} has an approximately linear dependence on $\sqrt{t_c}$, as shown in Fig. 7. In contrast, the ratio q_{in}/q_c is independent of potential and t_c except at very short charging times. The fact that this ratio lies between 0.02 and 0.03 (t_c>1 s) indicates that only about 2%-3% of the hydrogen atoms formed during charging enter the metal.

H_2SO_4. The electrode surface turned grey during the measurements, probably as a result of etching of the metal, and became extensively covered by hydrogen bubbles even at relatively low overpotentials (-0.15 V). These two factors, especially surface blocking by the bubbles, were assumed to be the cause of meaningless values observed for q_a. The anomalies in q_a precluded attempts to obtain k_a and J for the steel in this electrolyte.

NaCl/HCl. In this electrolyte, the surfaces of both steel specimens exhibited a blue tarnishing characteristic of interference effects associated with thin films. The formation of a film may have been due to the increase in pH at the electrode surface because of the unbuffered nature of the electrolyte; if the concentration of H^+ at the electrode surface during reduction became low enough, the pH would approach neutral and, with the reduction of H_2O, even become alkaline.

The errors in q_a caused by the formation of a film are thought to be responsible for some unexpected features in the behavior of k_a. Values of k_a and J for the steel in acidified NaCl are shown in Table 7, and it is evident that k_a changes erratically with potential, especially for the HRC 53 specimen. Moreover, k_a for the HRC 53 steel at the higher overpotentials is approximately twice as large as that for the HRC 41 specimen, and the average value of k_a for HRC 53 steel is 0.042 s^{-1}, in comparison with 0.026 s^{-1} for the lower strength steel. Finally, k_a for both specimens is high in comparison with the values obtained for steel in the acetate buffer of the same bulk pH as the NaCl/HCl solution.

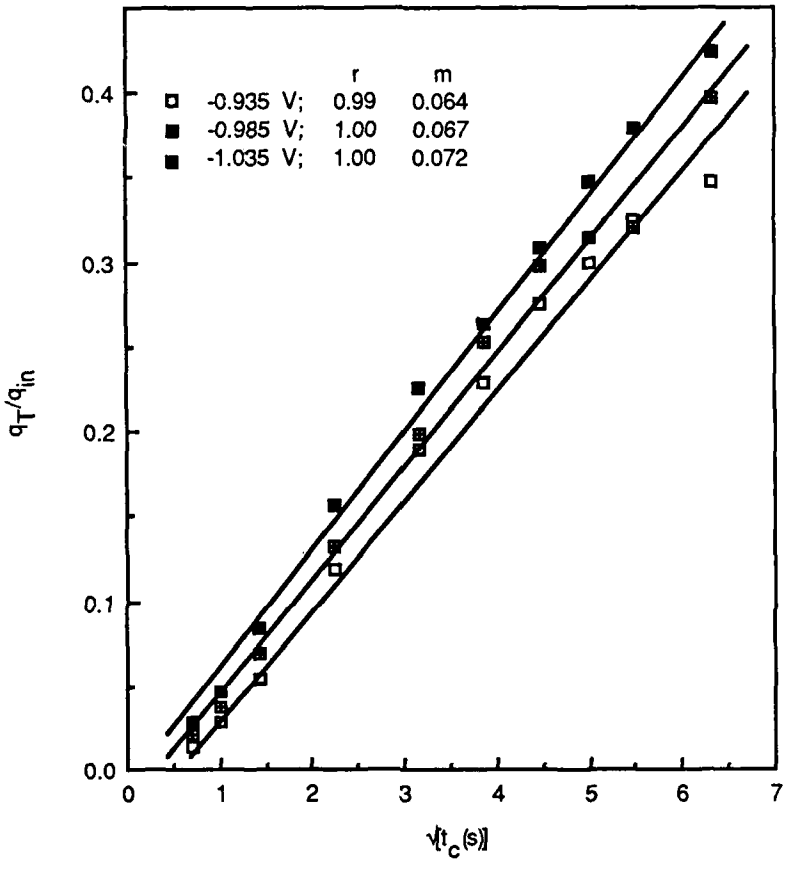

Figure 7. Dependence of trapped charge /ingress charge on charging time for 4340 steel HRC 53 in acetate buffer.

Table 7

INTERFACIAL FLUX AND TRAPPING CONSTANTS FOR 4340 STEEL IN NaCl/HCl

Type	η (V)	J (nmol cm^{-2} s^{-1})	k_a (s^{-1})
HRC 41	-0.25	0.89	0.036
	-0.30	1.14	0.028
	-0.35	1.13	0.019
	-0.40	1.43	0.029
	-0.50	1.55	0.019
HRC 53	-0.25	0.44	0.017
	-0.30	0.75	0.030
	-0.35	1.48	0.048
	-0.40	2.08	0.061
	-0.50	3.92	0.055

Phosphate. The surface of the steel developed a dark area, which suggested either etching or the formation of a film, and although trapping constants could be obtained, they varied randomly with increasing overpotential, as shown in Table 8. As with the NaCl/HCl solution, the average values of k_a (0.043 s^{-1} for HRC 41 and 0.032 s^{-1} for HRC 53) are high compared with those for the acetate buffer.

Table 8

INTERFACIAL FLUX AND TRAPPING CONSTANTS FOR 4340 STEEL IN PHOSPHATE

Type	η (V)	J (nmol cm^{-2} s^{-1})	k_a (s^{-1})
HRC 41	-0.25	1.41	0.057
	-0.30	1.82	0.020
	-0.35	3.62	0.046
	-0.40	1.43	0.049
HRC 53	-0.25	0.70	0.019
	-0.30	1.90	0.017
	-0.35	5.74	0.052
	-0.40	7.51	0.040

Bicarbonate. The electrode surface generally developed specks and often patches of blue tarnish typical of interference films. In some cases, tarnishing was not visible but the rate constants for the apparently untarnished electrodes fell within the range of those for tarnished electrodes. Moreover, the extent of visible tarnishing had little discernible effect on the trapping constant; that is, the results were within the limits of experimental error. Table 9 shows the values of k_a and J obtained for electrodes that showed a typical amount of tarnishing. Again, the average values of k_a (0.028 s^{-1} for HRC 41 and 0.050 s^{-1} for HRC 53) were higher than the corresponding results obtained with acetate.

Table 9

INTERFACIAL FLUX AND TRAPPING CONSTANTS FOR 4340 STEEL IN BICARBONATE

Type	η (V)	J (nmol cm^{-2} s^{-1})	k_a (s^{-1})
HRC 41	-0.50	0.54	0.019
	-0.55	0.79	0.038
	-0.60	0.71	0.025
	-0.65	0.86	0.030
HRC 53	-0.50	1.54	0.048
	-0.55	1.52	0.070
	-0.35	1.38	0.045
	-0.40	1.36	0.035

Monel K500

At sufficiently negative overpotentials, the open-circuit potential of the Monel in all electrolytes except H_2SO_4 shifted to more negative values during the range of charging times used and extensive bubble formation occurred. The shift in E_{oc} probably reflected reduction of an oxide film on the alloy surface; the implication is that at lower values of η, the reduction of H^+ and the subsequent entry of H atoms into the metal occurred on an oxide-covered surface.

Acetate. The anodic charge associated with oxidation of the adsorbed layer of hydrogen was again negligible; in this case, $q_{ads} \approx 7 \times 10^{-4}$ mC cm^{-2}. Values of the interfacial flux and trapping constant determined from q_a data for charging times from 10 to 40 s are given in Table 10.

Table 10

INTERFACIAL FLUX AND TRAPPING CONSTANTS FOR MONEL K500 IN ACETATE

Type	η (V)	J (nmol cm^{-2} s^{-1})	k_a (s^{-1})
AR	-0.65	0.15	0.027
	-0.70	0.18	0.027
	-0.75	0.18	0.019
	-0.80	0.21	0.027
HRC 35	-0.65	0.12	0.016
	-0.70	0.17	0.018
	-0.75	0.17	0.012

For both Monel specimens, the results exhibit similar patterns to those for 4340 steel: (1) k_a is essentially independent of E_c. (2) The flux increases with η, but not to the same extent as it does for 4340 steel. Even at the high overpotentials used for the Monel, the values of J are smaller than those for the steel, presumably because of the effect of the film.

Values of Q' calculated using the appropriate values of k_a and J for charging times from 0.5 to 40 s show good agreement with the corresponding experimental results, as shown for the Monel AR and η = -0.8 V [E_c = -0.905 V (SCE)] in Fig. 8. The difference between the two sets of data at short charging times probably reflects the influence of changes in the cathodic current in its early stages (see below) rather than a dependence of k and J on t_c. In addition, the precision of the q_a data for each potential was undoubtedly affected by small variations of up to 15 mV observed in E_{oc} over the range of t_c and particularly by the more pronounced changes in E_{oc} at higher overpotentials, as noted above.

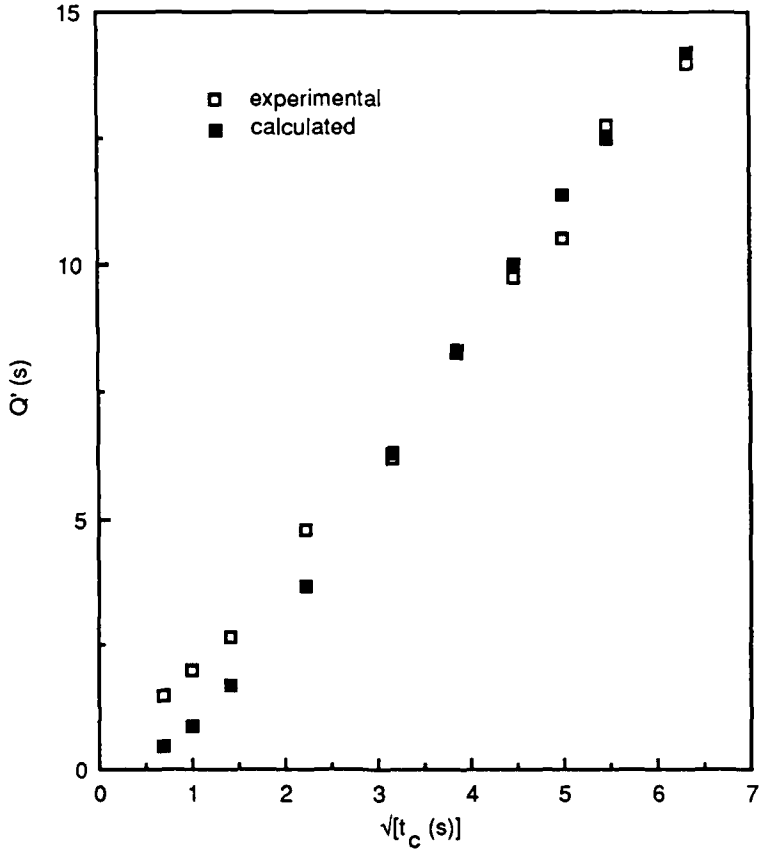

Figure 8. Comparison of anodic charge data for Monel K500 AR in acetate buffer.

E_c = -0.905 V (SCE)

In view of the limitations on the precision of the data, the value of k_a is probably quite similar for the two specimens despite the apparent difference between the two sets of experimental results shown in Table 10. Indeed, results for the aged Monel (HRC 35) in the other electrolytes (see below) give an average value for k_a of $0.022 \pm 0.007\ s^{-1}$. Therefore, the actual k_a for both Monel AR and HRC 35 in acetate was taken as the average of their derived values in Table 10: 0.025 and $0.015\ s^{-1}$ (averaged), respectively. The resulting average value for the two specimens is $0.020 \pm 0.005\ s^{-1}$, which is consistent with the values of k_a for the other solutions. Because k_a appeared to be similar for the two specimens, only the heat-treated alloy was used with the other electrolytes.

Values of the various charge parameters for Monel AR charged at $\eta = -0.8$ V are shown in Table 11. As with the steel, the cathodic current was shown to be essentially constant from the linear relationship between q_c and t_c (Fig. 9). The small deviation from linearity for t_c <2 s can be attributed to the greater effect of initial changes in the cathodic current for these charging times. Likewise, q_{in} conforms to the predicted linear dependence on t_c (Fig. 6), giving a slope of 19.4 $\mu C\ cm^{-2}\ s^{-1}$ for $\eta = -0.8$ V. This slope corresponds to a flux of 0.20 $nmol\ cm^{-2}\ s^{-1}$ as used in equation (12). As with the HRC 53 steel, the ratio q_T/q_{in} increases with t_c and q_{in}/q_c is essentially constant, with a value of 0.02-0.03 over the range 2 to 40 s. The remarkable characteristic of q_{in}/q_c is that it does not vary with either the type of alloy (4340 steel or Monel K500) or the potential; this invariance implies that q_{in} and q_c have a similar potential dependence to each other for the two alloys.

Table 11

CHARGE PARAMETERS[a] FOR MONEL AR IN ACETATE[b]

t_c (s)	q_T	q_a	q_{in}	q_T/q_{in}	q_c	$\lvert q_{in}/q_c \rvert$
0.5	0.001	0.030	0.031	0.029	-0.71	0.043
1	0.002	0.041	0.043	0.057	-1.38	0.032
2	0.007	0.056	0.063	0.111	-2.40	0.026
5	0.027	0.101	0.128	0.213	-5.26	0.024
10	0.075	0.126	0.201	0.374	-9.30	0.022
15	0.135	0.168	0.303	0.445	-13.25	0.023
20	0.202	0.198	0.400	0.505	-17.47	0.023
25	0.276	0.213	0.489	0.565	-21.24	0.023
30	0.355	0.259	0.614	0.578	-24.98	0.025
40	0.523	0.283	0.806	0.649	-31.77	0.025

[a] The units of charge are mC/cm^2.

[b] η = -0.8 V; used $k_a = 0.027\ s^{-1}$, $J = 0.21$ nmol $cm^{-2}\ s^{-1}$ for q_T.

H_2SO_4. The values of q_a were low and showed negligible change with t_c, even up to an overpotential of -1.3 V; this implies that essentially no hydrogen entered the metal in this electrolyte at the charging potentials used. In addition, the open-circuit potential for the Monel in H_2SO_4 did not show the distinct negative shift that occurred in the other electrolytes at high overpotentials. This suggests that a surface film did not form on the Monel in the H_2SO_4, and therefore the behavior of q_a can be explained by the low exchange current densities for hydrogen evolution reported for nickel and copper [log i_o (A cm^{-2}) = -5.25 for Ni and -7.8 for Cu in 0.5 M H_2SO_4].[17] Moreover, the hydrogen coverage on a copper surface is reported to be low in the steady state.[18] Thus, despite the use of high overpotentials, the adsorbed hydrogen and therefore the interfacial flux on the Monel surface in H_2SO_4 is insufficient to allow absorption of a significant quantity of

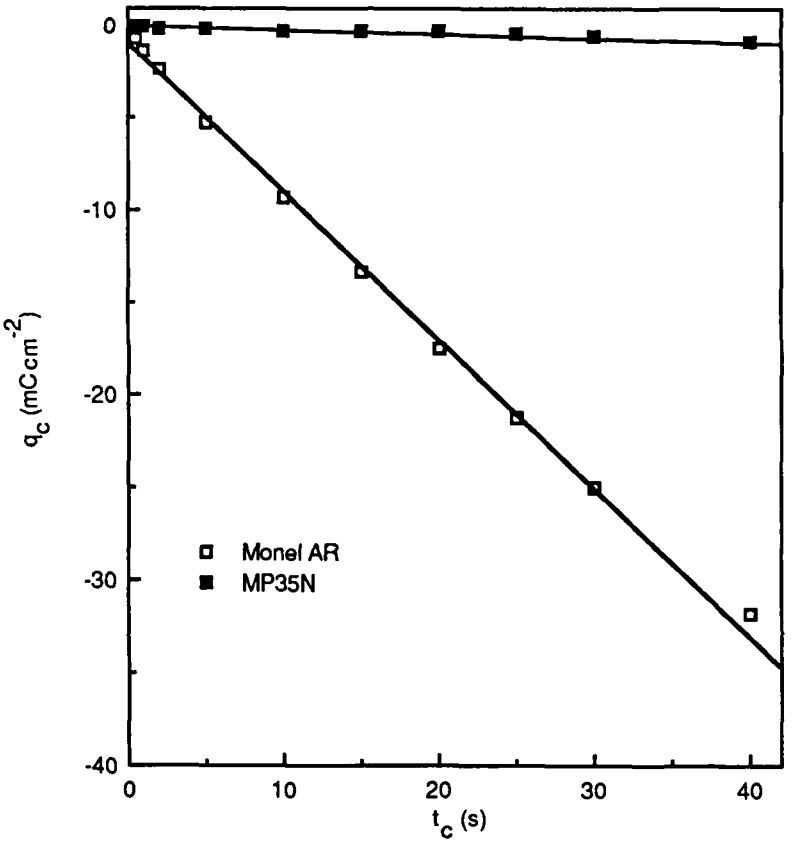

Figure 9. Dependence of cathodic charge on charging time for Monel K500 AR and MP35N in acetate buffer.

E_c (SCE) = -0.905 V for Monel; -0.425 V for MP35N

hydrogen.

NaCl/HCl. The trapping constants for the HRC 35 specimen showed some scatter over the range of overpotentials, as shown in Table 12, but the mean value of 0.029 s^{-1} was consistent with that for the acetate solution.

Table 12

INTERFACIAL FLUX AND TRAPPING CONSTANTS FOR MONEL K500 HRC 35 IN NaCl/HCl

η (V)	J (nmol cm^{-2} s^{-1})	k_a (s^{-1})
-0.60	0.16	0.028
-0.65	0.23	0.034
-0.70	0.29	0.040
-0.75	0.26	0.019
-0.80	0.41	0.016
-0.85	0.69	0.023
-0.90	1.31	0.057
-0.95	0.88	0.015

Phosphate. The values of k_a for the HRC 35 specimen are given in Table 13. They show somewhat less scatter than those for the acidified NaCl, but they still vary from 0.010 to 0.023 s^{-1}. The mean value is 0.017 s^{-1}.

Table 13

INTERFACIAL FLUX AND TRAPPING CONSTANTS FOR MONEL K500 HRC 35 IN PHOSPHATE

η (V)	J (nmol cm^{-2} s^{-1})	k_a (s^{-1})
-0.60	0.19	0.020
-0.65	0.18	0.014
-0.70	0.22	0.014
-0.75	0.23	0.018
-0.80	0.23	0.019
-0.85	0.20	0.010
-0.90	0.27	0.021
-0.95	0.29	0.023

Bicarbonate. The values of k_a for Monel HRC 35 in the bicarbonate buffer (Table 14) are similar to those in the phosphate buffer. The mean value, 0.019 s^{-1}, is also similar.

Table 14

INTERFACIAL FLUX AND TRAPPING CONSTANTS FOR MONEL K500 HRC 35 IN BICARBONATE

η (V)	J (nmol cm^{-2} s^{-1})	k_a (s^{-1})
-0.60	0.43	0.024
-0.65	0.51	0.023
-0.70	0.50	0.009
-0.75	0.89	0.022
-0.80	0.85	0.017

MP35N

The behavior of this alloy was similar to but more marked than that of the Monel. The open-circuit potential for MP35N in all electrolytes drifted considerably over the range of t_c values at each potential. During the early stages of immersion, E_{oc} showed a net positive drift over the range of charging times and charging potentials, presumably as a result of passivation of the freshly-polished surface of the electrode. The presence of a film was further indicated by a substantial negative shift in E_{oc} over the range of charging times at sufficiently high cathodic overpotentials and by an increase in the values of q_a far greater for these overpotentials than for lower overpotentials. Thus, as with the Monel, it is evident that hydrogen enters MP35N across a surface film, even up to relatively high overpotentials.

A change in E_{oc} means that, for a given η, E_c is not constant over the range of charging times. Rather than sample E_{oc} for each charging time, it could have been sampled only at the start of each new overpotential, so that E_{oc} and therefore E_c were the same for each t_c. However, this approach was thought not to reflect the true corrosion state of the alloy during the series of hydrogen charging/discharging times for a given potential. In contrast, the method used was considered to relate more closely to the actual corrosion condition at <u>any</u> time of exposure.

The drift in E_{oc} (positive or negative) limited the data that were valid in terms of the generalized PDP conditions were somewhat restricted, but the flux control model was found to be applicable in all cases where analysis was possible.

<u>Acetate</u>. The anodic charge was again shown to be almost entirely associated with absorbed hydrogen ($q_{ads} \approx 10^{-3}$ mC cm^{-2}). Table 15 shows the values of J and k_a determined for charging times from 10 to 40 s. The value of k_a is approximately constant for the three lower values of η but decreases as E_c becomes more negative. The open-circuit potential exhibited a significant negative shift at η = -0.55 V and an even greater one at -0.6 V

(Fig. 10). Therefore, the decrease in k_a is believed to be an artifact resulting from partial film reduction/repassivation, which inflates the value of q_a. The increased charge makes it appear that less hydrogen is trapped in the metal during egress, so there is an apparent decrease in k_a. The average value of 0.026 s^{-1} for k_a taken over η = -0.35 to -0.45 V is considered to be reliable for MP35N.

Table 15

INTERFACIAL FLUX AND TRAPPING CONSTANTS FOR MP35N FOR ACETATE

η (V)	J (nmol cm^{-2} s^{-1})	k_a (s^{-1})
-0.35	0.04	0.029
-0.40	0.05	0.024
-0.45	0.08	0.026
-0.50	0.08	0.004
-0.55	0.19	0.0002

As for the Monel, the presence of the film apparently results in lower values of J than those for the steel. Values of Q' calculated using the appropriate values of k_a and J for charging times from 0.5 to 40 s correspond well with the experimental results, as shown for η = -0.40 V [E_c = -0.425 V (SCE)] in Fig. 11. The difference between the two sets of data at short charging times is again probably caused by changes in the cathodic current in its early stages and small variations in E_{oc} rather than a dependence of k and J on t_c.

Values of the charge parameters for MP35N charged at η = -0.40 V are shown in Table 16. Both q_{in} (Fig. 6) and q_c (Fig. 9) follow the predicted

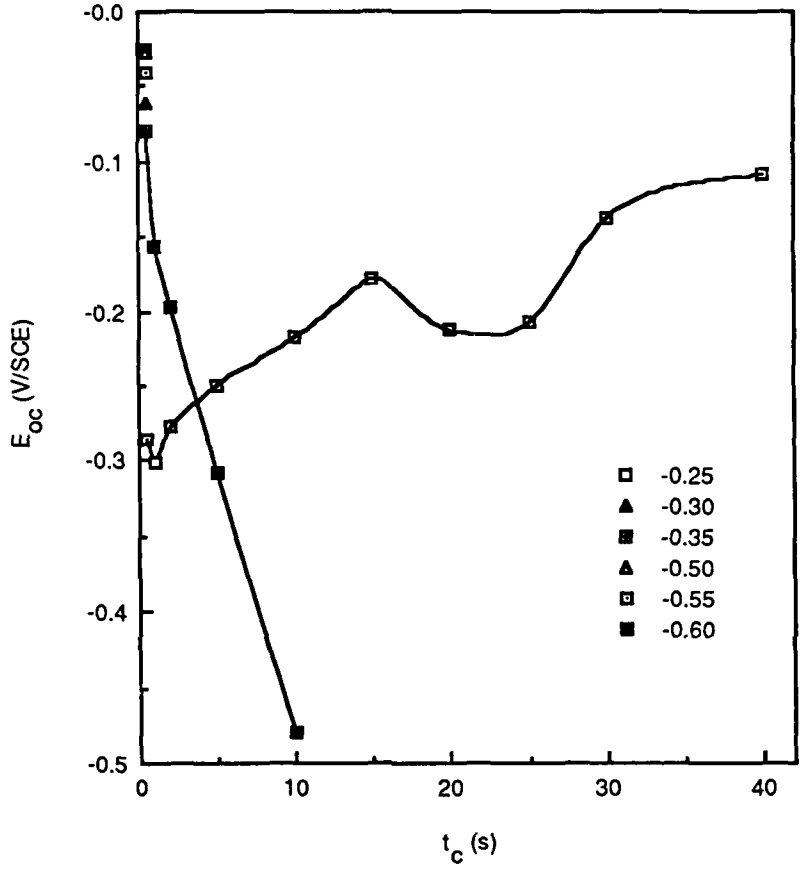

Figure 10. Variation of open-circuit potential with charging time for MP35N in acetate buffer.

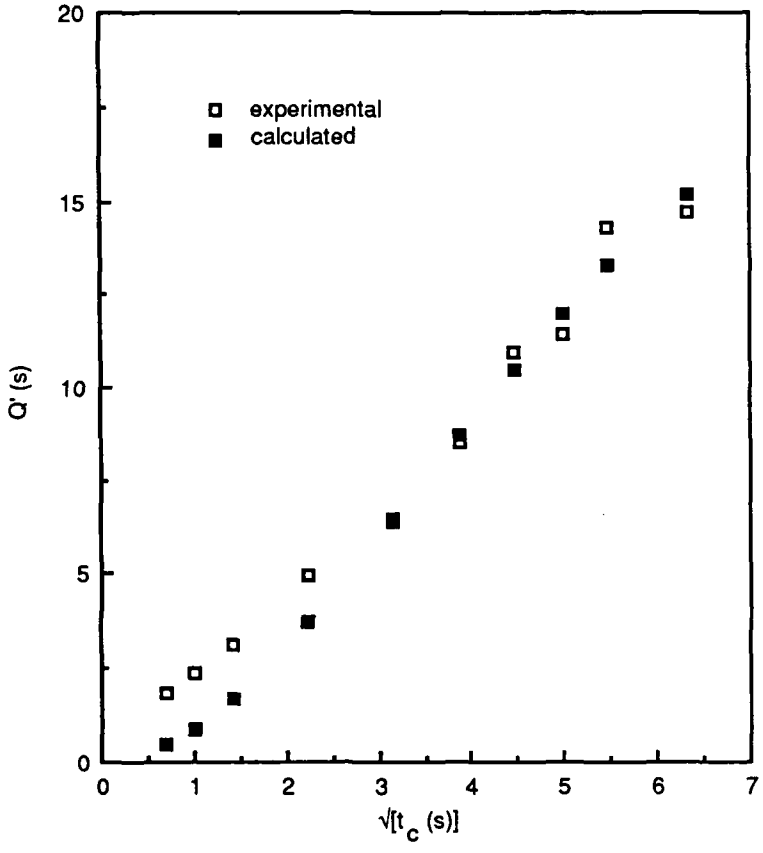

Figure 11. Comparison of anodic charge data for MP35N in acetate buffer.

E_c = -0.425 V(SCE)

linear dependence on t_c. The slope of the q_{in}/t_c plot for η = -0.40 V is 4.5 μC cm^{-2} s^{-1}, corresponding to the value of J (0.047 nmol cm^{-2} s^{-1}) used in equation (12). As for the other two alloys, q_T/q_{in} increases with t_c and q_{in}/q_c is roughly independent of t_c, but the values of q_{in}/q_c for MP35N are an order of magnitude higher than those for the steel and Monel.

Table 16

CHARGE PARAMETERS[a] FOR MP35N IN ACETATE[b]

t_c (s)	q_T	q_a	q_{in}	q_T/q_{in}	q_c	$\lvert q_{in}/q_c \rvert$
0.5	0.000	0.010	0.010	0.020	-0.03	0.340
1	0.001	0.016	0.017	0.034	-0.04	0.414
2	0.002	0.017	0.019	0.086	-0.06	0.310
5	0.006	0.028	0.034	0.183	-0.12	0.285
10	0.017	0.031	0.048	0.358	-0.23	0.210
15	0.031	0.041	0.072	0.431	-0.29	0.248
20	0.047	0.053	0.100	0.468	-0.29	0.344
25	0.064	0.047	0.111	0.576	-0.38	0.292
30	0.082	0.069	0.151	0.543	-0.50	0.302
40	0.121	0.071	0.192	0.631	-0.86	0.224

[a] The units of charge are mC/cm^2.

[b] η = -0.4 V; used k_a = 0.024 s^{-1}, J = 0.05 nmol cm^{-2} s^{-1} for q_T.

H_2SO_4. The values of k_a and J are given in Table 17. The decrease in k_a for η = -0.55 V is accompanied by a marked negative shift in E_{oc} (Fig. 12) that suggests that q_a is affected by repassivation following partial reduction during t_c at this overpotential. As with the steel and Monel, the values of k_a were derived using q_a data for charging times from 10 to 40 s, but it is evident that E_{oc} is not stable even over this t_c range for the other three

overpotentials. Nevertheless, only the result for $\eta = -0.55$ V was excluded in calculating the average value of k_a, which was found to be 0.031 s^{-1}.

Table 17

INTERFACIAL FLUX AND TRAPPING CONSTANTS FOR MP35N IN H_2SO_4

η (V)	J (nmol cm^{-2} s^{-1})	k_a (s^{-1})
-0.40	0.41	0.042
-0.45	0.29	0.021
-0.50	0.25	0.029
-0.55	0.12	0.008

NaCl/HCl. The values of k_a and J are given in Table 18, and it is clear that k_a is subject to some scatter.

Table 18

INTERFACIAL FLUX AND TRAPPING CONSTANTS FOR MP35N IN NaCl/HCl

η (V)	J (nmol cm^{-2} s^{-1})	k_a (s^{-1})
-0.35	0.18	0.019
-0.40	0.33	0.070
-0.45	0.18	0.015
-0.50	0.30	0.042
-0.55	0.35	0.041
-0.60	0.32	0.032
-0.65	0.33	0.024

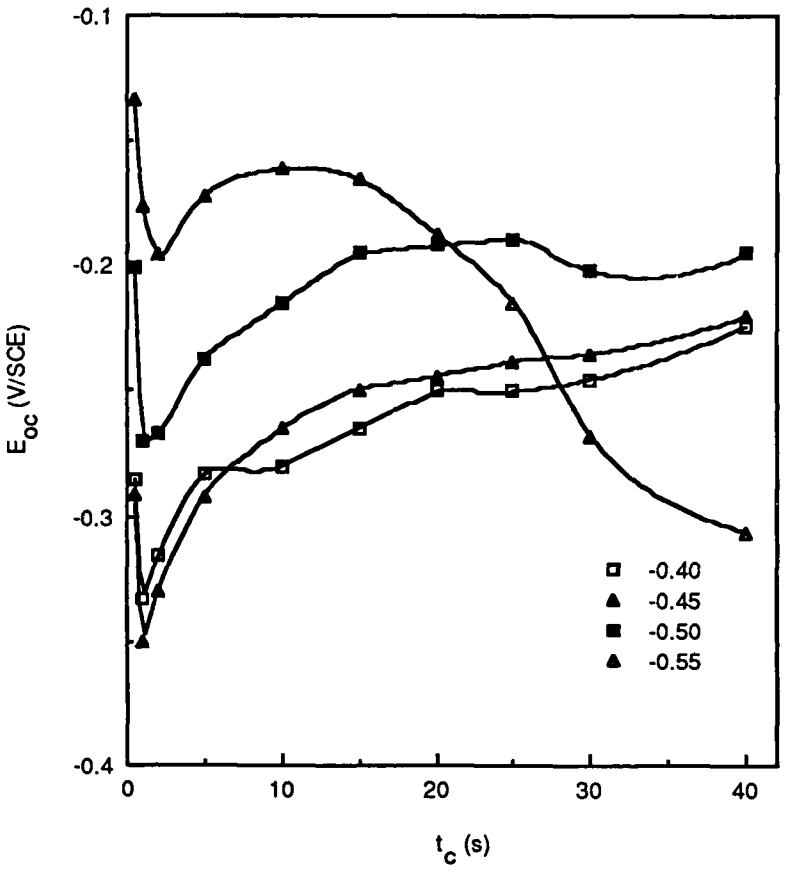

Figure 12. Variation of open-circuit potential with charging time for MP35N in sulfuric acid.

At η = -0.65 V, E_{oc} begins to have a negative shift over the range of t_c, as shown in Fig. 13, and at -0.7 V, many small bubbles appeared on the surface. These observations suggested that the data for -0.65 V were not reliable for analysis in terms of the hydrogen ingress models, so the average value of k_a was calculated excluding the result for -0.65 V. The average value of k_a was found to be 0.037 s^{-1}.

Phosphate. The variation in open-circuit potential was relatively small over the range of t_c values (10-40 s) used in the data analysis (Fig. 14). However, because q_a generally varied in an inconsistent manner with t_c, reliable values of k_a could not be extracted.

Bicarbonate. The values of J and k_a are shown in Table 19. The data for η = -0.55 V could not be analyzed because q_a decreased as t_c increased, probably as a result of the relatively large change in E_{oc} with t_c for this overpotential (Fig. 15). The value of k_a for η = -0.65 V is undoubtedly influenced by reduction of the film, as reflected by the shift in E_{oc}. *Accordingly, only the results for -0.50 and -0.60 V were used to determine the* average value of k_a, which was calculated to be 0.058 s^{-1}.

Table 19

INTERFACIAL FLUX AND TRAPPING CONSTANTS FOR MP35N IN BICARBONATE

η (V)	J (nmol cm^{-2} s^{-1})	k_a (s^{-1})
-0.50	1.08	0.056
-0.55	n	n
-0.60	0.49	0.060
-0.65	0.42	0.006

n = data not analyzable

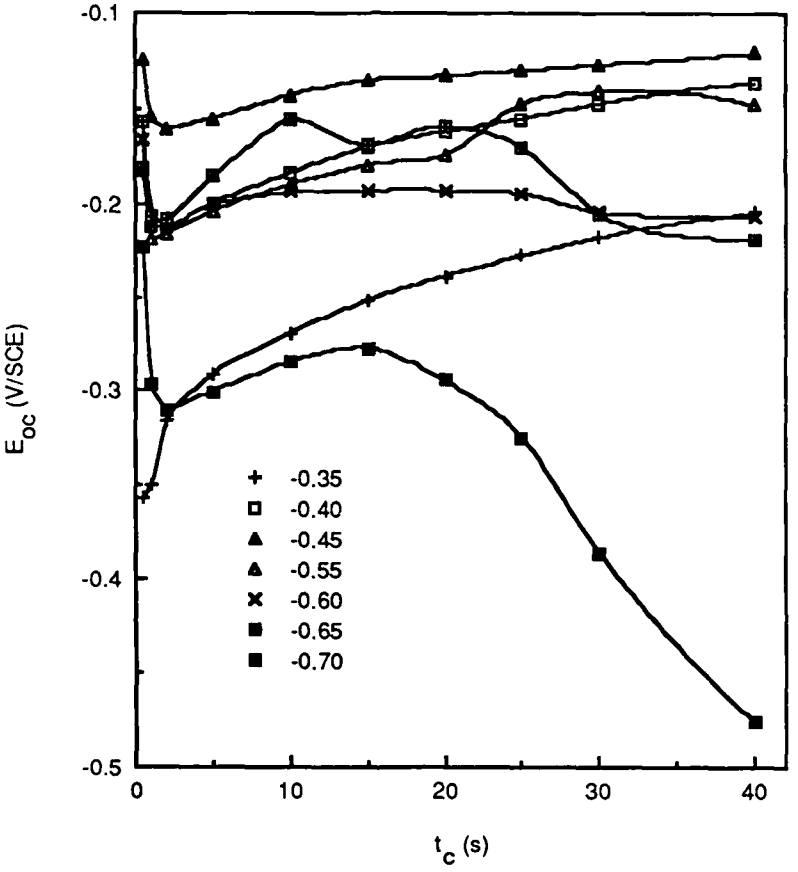

Figure 13. Variation of open-circuit potential with charging time for MP35N in NaCl/HCl.

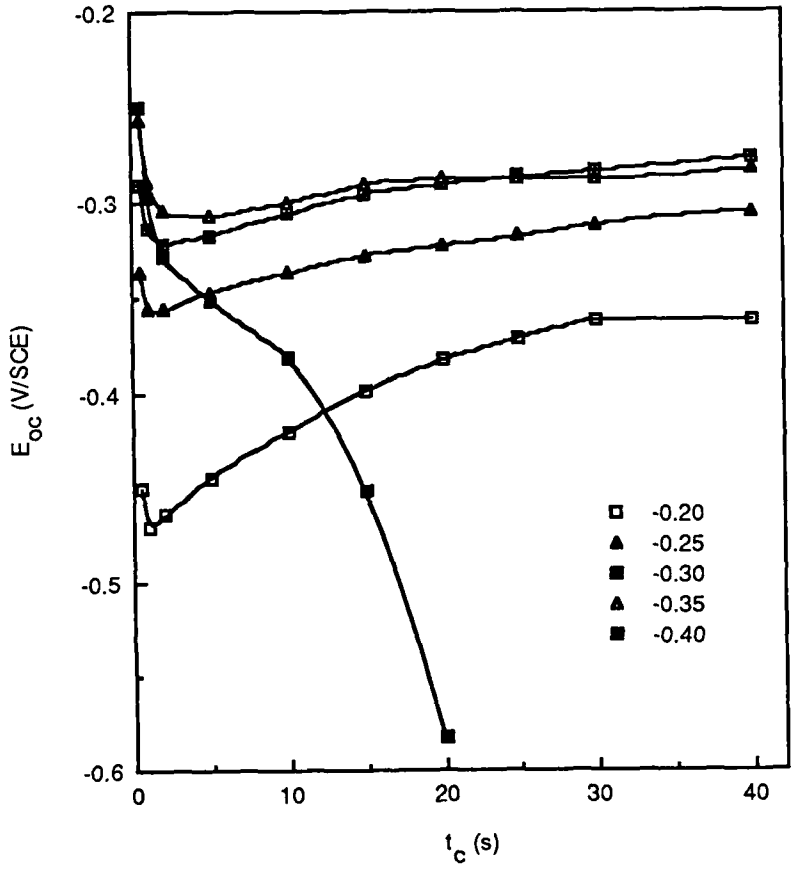

Figure 14. Variation of open-circuit potential with charging time for MP35N in phosphate buffer.

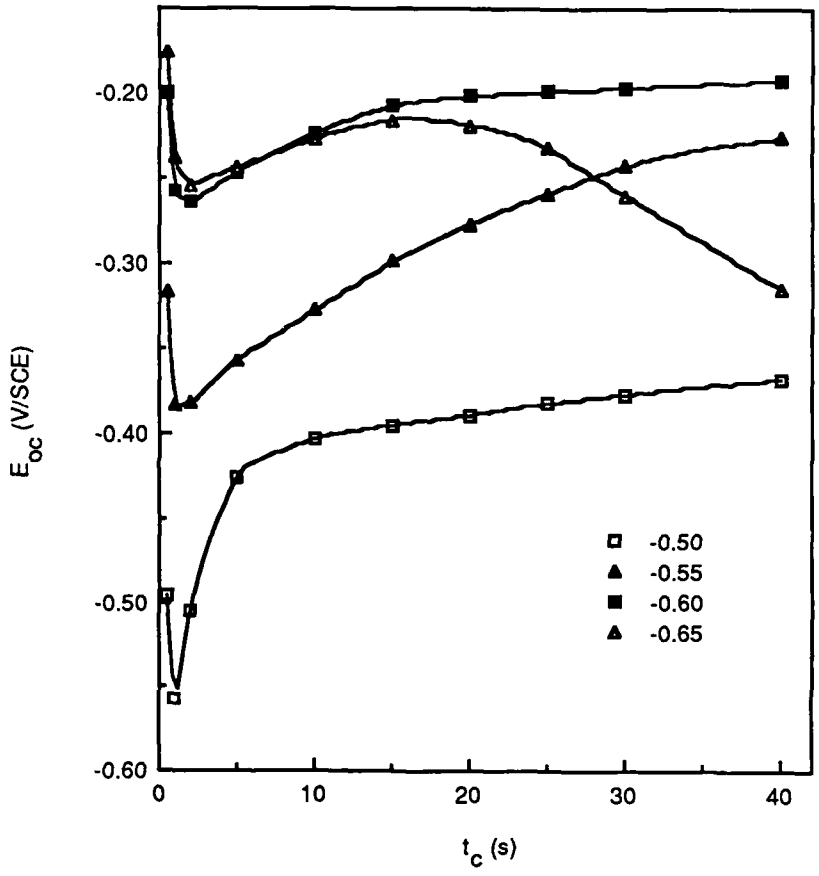

Figure 15. Variation of open-circuit potential with charging time for MP35N in bicarbonate buffer.

DISCUSSION

4340 Steel

The average values of k_a for each electrolyte are summarized in Table 20.

Table 20

AVERAGE VALUES OF k_a FOR 4340 STEEL

Electrolyte	k_a (s^{-1}) HRC 41	HRC 53	Surface Condition
Acetate	0.008	0.008	No visible change
H_2SO_4	n	n	Etching, bubbles
NaCl/HCl	0.026	0.042	Blue tarnishing
Phosphate	0.043	0.032	Dark areas
Bicarbonate	0.028	0.050	Blue tarnishing

n = not obtainable

The trapping constants should be independent of pH because they are determined only by internal structural features of the alloys, but the interfacial flux of hydrogen across the metal surface should exhibit some variation with pH. However, because the electrode surface was subject to dissolution or film formation in all electrolytes except acetate, only the data for the acetate buffer are considered valid in terms of the hydrogen ingress model.

The irreversible trapping constant (k) for 4340 steel in the acetate can be obtained from the value of k_a by using diffusivity data to evaluate the equilibrium constant (K_r). The apparent diffusivity (D_a) for hydrogen in HRC 50 electroslag remelted (ESR) 4340 steel was found from membrane

permeation experiments[19] to be ~10^{-7} cm^2 s^{-1}. The difference in diffusivity between this ESR steel and the VAR-produced specimen used in this study is assumed to be small enough to ignore; that is, it is believed to be at least within the same order of magnitude. Data reported for D_L in pure iron show considerable variation, but a value of about 5 x 10^{-5} cm^2 s^{-1} at 25°C appears to be reliable.[20,21] Using these values for D_a and D_L, K_r was calculated to be approximately 500, and therefore k was 4 s^{-1}.

The trapping constant can be regarded as the mean trapping frequency of a single hydrogen atom in the metal lattice and can be related to the trap density on the basis of a simple model[4] involving spherical traps of radius d and surface area $4\pi d^2$. This model yields the following expression for k in terms of the concentration (N_i) of traps:

$$k = 4\pi d^2 N_i D_L / a \qquad (14)$$

where a is the diameter of the metal atom. The diameter of the iron atom is 248 pm but a value for d is also required to estimate N_i. This in turn presupposes a knowledge of potential irreversible traps. Such traps have been defined[22] to have a binding energy for hydrogen of ≥60 kJ mol^{-1}, and thermal analysis data[15] for 4340 steel showed that MnS inclusions in the steel have a binding energy of 72 kJ mol^{-1}.

The MnS inclusions in the test specimen were ellipsoidal, so assuming that the traps in the above model are spherical is somewhat of an approximation. However, using the value of 9.2 μm for the mean radius of the MnS inclusions, the density of traps was calculated to be 2 x 10^8 m^{-3}. In view of the assumed spherical shape for the traps and the MnS inclusions, this value is in reasonable agreement with the actual concentration of inclusions, 2 x 10^9 m^{-3}. The inclusion content should not be altered by heat treatment, and in fact, the value of N_i is the same for both the HRC 41 and HRC 53 specimens, further indicating that the irreversible traps determined from the PDP measurements are stable entities such as MnS inclusions.

Other irreversible traps such as Fe_3C and TiC interfaces could participate, but on the basis of the value of N_i, they appear to have only a relatively minor role. Although the trap density was calculated using the mean radius of MnS inclusions, the value of d would have to be unreasonably small (0.01-0.1 pm, i.e., 3-4 orders of magnitude smaller than the radius of the iron atom) for k to equal 4 s^{-1} at a value of N_i that approached the typical levels of Fe_3C and TiC interfaces in steels (10^{24}-10^{25} m^{-3}).[10]

Monel K500

The average values of k_a for the Monel and MP35N are shown in Table 21 The values for the Monel are independent of pH, so the hydrogen ingress model appears to be valid irrespective of the electrolyte provided that the state of the electrode surface (in this case, the state of the oxide film) is not affected by either a change of electrolyte or cathodic charging.

Table 21

AVERAGE VALUES OF k_a FOR MONEL K500 AND MP35N

	k_a (s^{-1})	
Electrolyte	Monel	MP35N
Acetate	0.020[a]	0.027
H_2SO_4	b	0.031
NaCl/HCl	0.029	0.037
Phosphate	0.017	c
Bicarbonate	0.019	0.058

[a] Averaged for AR and aged specimens.

[b] q_a was essentially invariant with t_c.

[c] Anomalous results.

The average value of k_a for the Monel in the different electrolytes is $0.021\ s^{-1}$. Evaluation of the irreversible trapping constant (k) from the value of k_a requires diffusivity data for the pure Ni-Cu alloy to obtain D_L and also for Monel K500 to obtain D_a; the effect of defects such as vacancies and edge dislocations on hydrogen diffusion in an fcc lattice is assumed to be small enough to ignore (discussed above), and therefore the minor elements rather than defects in the Monel are believed to determine the reversible trapping behavior.

The diffusivity of hydrogen determined from membrane permeation experiments is $3 \times 10^{-10}\ cm^2\ s^{-1}$ in 30 at.% Cu-70 at.% Ni[23] at 25°C and $1.48 \times 10^{-10}\ cm^2\ s^{-1}$ in cold worked and aged Monel K500 (assumed to be at ambient temperature).[24] Although the levels of Cu and Ni differ slightly in the Ni-Cu alloy and the Monel, the error in using the diffusivity of the Ni-Cu alloy for D_L is considered to be negligible. Accordingly, using these data for D_L and D_a, K_r is found to be ~2 and therefore, the value of k is $0.042\ s^{-1}$.

Hydrogen embrittlement in Ni-Cu base alloys is known to be assisted by sulfur segregated at grain boundaries.[25] If the primary irreversible trap in both Monel specimens is assumed to be sulfur (considered as the atomic form in solid solution rather than as a copper-nickel sulfide), then the atomic radius of sulfur can be used for d. The value of a is determined from the weighted mean atomic diameter of Cu (256 pm) and Ni (250 pm). Therefore, with $d = 104$ pm, $a = 252$ pm, $D_L = 3 \times 10^{-10}\ cm^2\ s^{-1}$, and $k = 0.042\ s^{-1}$, the density of irreversible traps in the Monel (AR and HRC 35) is found to be $2.6 \times 10^{21}\ m^{-3}$. The actual concentration of sulfur, calculated from the density of Monel K500 ($8.43\ g\ cm^{-3}$) and the wt% data for sulfur in Table 1, is 1.6×10^{24} S atoms m^{-3} for the AR Monel. This value is also assumed to be valid for the aged Monel although the distribution of sulfur will probably be different due because of segregation at grain boundaries.

The difference of three orders of magnitude between the value of N_i and

the concentration of sulfur atoms may indicate that the primary irreversible traps in the Monel are not associated with sulfur. Other minor elements, such as Fe, C, and Mn, could well be responsible for other types of irreversible traps. On the other hand, the difference between the experimental and expected values of N_i could result from the segregation of sulfur.

The concentration of sulfur segregated at grain boundaries can be considerably higher than that in the bulk, so that the traps at grain boundaries are likely to consist of sulfur clustered either in the elemental form or, more probably, as sulfides. Hydrogen as well as sulfur is known[26] to segregate to the grain boundaries in nickel. Therefore, sulfur clusters are expected to be the traps predominantly encountered by the hydrogen, so that the value of N_i for the Monel in fact probably reflects these clusters. Thus, sulfur, either as the sulfide or in the elemental form, still appears likely to be the principal site for irreversible trapping in the Monel.

The surface film also influences the diffusion and trapping behavior of the underlying alloy. The hydrogen atoms generated on the surface of the film-covered alloy clearly must diffuse through the film before entering the alloy. However, almost all the diffusion distance can be shown to lie in the metal rather than in the film. The mean distance, χ, that the hydrogen diffuses into a metal (assuming that no interference with the diffusion process occurs) is given by

$$\chi = \sqrt{(2D_L t_c)} \tag{15}$$

The diffusion of hydrogen through the oxide as well as through the alloy during the charging period is probably not accurately reflected by the diffusivity for the alloy alone. Nevertheless, the diffusivity of hydrogen through the film is expected to be low, and therefore could be comparable to the hydrogen diffusivity for the Monel; that is, they could be within an order of magnitude. Accordingly, if $D_L = 10^{-10}$ cm^2 s^{-1}, χ ranges from 0.45 to 0.89 μm for charging times from 10 to 40 s. The thickness of the oxide film

anodically formed on nickel in aqueous solutions is typically no more than 1-2 nm,[27-29] so if we assume a maximum thickness of 2 nm for the film on the Monel, only 0.2% to 0.4% of the diffusion distance involves the film for charging times from 40 s down to 10 s.

The distribution of sulfur in the oxide is likely to differ from that in the alloy, so that the mobile hydrogen will encounter most of the sulfur traps in one part of its overall diffusion distance. Thus, the experimentally determined trap density will be a weighted mean of the respective trap densities, N_m and N_f, for the metal and the film, or more precisely, of the respective number of traps encountered over each part of the diffusion distance, δ. A weighted form of the mean must be used because of the nonuniform concentration profile of diffusing hydrogen. The number of traps encountered over the diffusion distance in a material, j, is proportional to $N_j\delta_j$, so that N_i is assumed to be given as a weighted mean by the following expression:

$$N_i = [w_m N_m \delta_m + w_f N_f \delta_f] / [(\delta_m + \delta_f)(w_m + w_f)] \qquad (16)$$

where w_m and w_f are the weighting factors for the metal and film, respectively. If the weighted sulfur concentration in the film and therefore $w_f N_f$ is low enough, the film could contribute to the low value of the experimentally-determined trap density (N_i) in comparison with the expected trap density (N_m). However, because the fraction of the diffusion distance that involves the film is very small, the difference in sulfur distributions is probably a secondary effect.

MP35N

The average values of k_a for MP35N are listed in Table 21. Unlike the situation with the Monel, these values change with electrolyte. Some of this variation may result from shifts in the open-circuit potential over the range of charging times that arise from changes in the state of the alloy surface due to film formation (evident from the positive shift in E_{oc}) and then film

reduction (evident from the negative shift in E_{oc}). However, in several cases, such as η = -0.60 V in bicarbonate and η = -0.45 V in NaCl/HCl, the open-circuit potential was approximately constant with t_c but the values of k_a were quite different (0.060 s^{-1} and 0.015 s^{-1}, respectively). This suggests that k_a may depend on the nature of the electrolyte.

The trapping constant increases in the following order: acetate < H_2SO_4 < NaCl/HCl < bicarbonate. Except for acetate, this is also the order of increasing pH. However, as noted above, the acetate buffer is expected to provide a more constant supply of H^+ at the electrode surface than do the unbuffered H_2SO_4 and acidified NaCl, especially at the relatively low H^+ concentrations used. Thus, the variation in k_a with electrolyte suggests that k_a depends strictly on the interfacial pH, not the bulk pH. However, k_a is associated with a process (trapping) <u>within</u> the metal and should not vary with interfacial conditions.

An increase in pH would cause the reaction for H_2 formation to change from reduction of H^+ in acidic solutions to reduction of H_2O in neutral and alkaline solutions. However, although a change in reaction may well affect the amount of adsorbed hydrogen and therefore the flux of hydrogen across the surface, it would not be expected to influence k_a directly. The decrease in H^+ concentration with an increase in pH may have increased the time needed for the adsorbed layer of hydrogen to reach its steady state coverage and therefore the time needed for the ingress flux to become constant. Such behavior would violate the condition of constant flux assumed for the hydrogen ingress model and may have been responsible for the apparent change in k_a, but if a constant flux were not rapidly attained on MP35N, the Monel should have behaved similarly and shown an increase in k_a; this was not the case.

A change in pH can also affect the stability of the surface film in terms of its thickness and composition, and this may provide an explanation for the change in k_a. At higher pH values up to moderate alkalinity (pH 9-10), the film is likely to be thicker, so that hydrogen atoms must diffuse through a

greater distance before entering the metal itself. Thus, the thicker the film, the more the hydrogen would be exposed to the type of traps in the film over its diffusion path. This argument assumes that the diffusivities of hydrogen in the film and the alloy are similar on the basis that the diffusivity for MP35N is low and therefore is probably comparable to the diffusivity for the film, which is also expected to be low.

The mean trap density for the metal and film is given by equation (16). If it is assumed that the diffusivities of hydrogen in the film and alloy are similar, the measured irreversible trapping constant can be represented by the following expression:

$$k = [w_m' k_m \delta_m + w_f' k_f \delta_f] / [(\delta_m + \delta_f)(w_m' + w_f')] \qquad (17)$$

where k_m and k_f are the irreversible trapping constants for the metal and film, respectively. Clearly, the measured irreversible trapping constant depends on the thickness of the film, and therefore the film thickness could account for the change in k_a with interfacial pH. The k_a for the Monel was found to be independent of pH, and this is consistent with previous work showing that the thickness of the passivating film on nickel is nearly independent of pH.[28]

Clearly, this explanation is somewhat speculative and more information is needed about the nature of the film on MP35N in the different electrolytes to show that there is in fact a significant change in its thickness. Nevertheless, if this explanation is valid, the trapping constant for the acetate should be least dependent on the film, and therefore, it should be a more reliable value with which to determine the density of the principal irreversible traps in the alloy itself. Furthermore, because the acetate has a relatively low interfacial pH, the time required for the flux to become constant is likely to be minimal. Accordingly, the value of k_a for the acetate has been used to calculate N_T below.

Evaluation of k from the value of k_a requires diffusivity data for the "pure" Co-Ni-Cr-Mo alloy and for MP35N. However, these data do not appear to be available for MP35N, and the most appropriate data for the pure alloy are for 50 at.% Co-50 at.% Ni, for which D_L is 5.5×10^{-11} cm^2 s^{-1} at 25°C;[23] because two other primary elements are present in MP35N, there may be a significant difference in diffusivity between the Co-Ni alloy and the quaternary base of MP35N. In the absence of diffusivity data for MP35N, minor elements, particularly those acting as reversible traps, were assumed to have little effect on the low diffusivity of hydrogen in the "pure" alloy lattice compared with the effect in iron, where the true lattice diffusivity is five orders of magnitude higher. On this basis, D_a was assumed to be approximately equal to D_L and therefore $k \approx k_a$.

The resistance of MP35N to hydrogen embrittlement has been correlated with the concentration of phosphorus and sulfur impurities segregated at its major crystallographic boundaries.[30] If the sulfur and phosphorus (in atomic form) are considered the primary irreversible traps, d can be taken as the mean atomic radius of sulfur (104 pm) and phosphorus (110 pm). Likewise, the value used for a is the mean diameter of Co (250 pm) and Ni (250 pm). Therefore, with d = 107 pm, a = 250 pm, $D_L = 5.5 \times 10^{-11}$ cm^2 s^{-1}, and $k = 0.026$ s^{-1}, N_i is 8.2×10^{21} m^{-3}.

The actual concentration of sulfur and phosphorus, calculated from the density of MP35N (8.43 g cm^{-3}) and the wt% data for these elements in Table 1, is 8.1×10^{24} S and P atoms m^{-3}. The difference of three orders of magnitude between the value of N_i and the concentration of sulfur and phosphorus atoms, as with the Monel, may indicate that these elements are not the primary irreversible traps. Like the Monel, MP35N contains other minor elements, such as Fe, C, and Mn, as well as S and P, that could be involved in irreversible traps. Still, as with the Monel, the difference is probably associated with sulfur, and phosphorus, clusters at grain boundaries providing the main traps encountered by the hydrogen. In addition, the surface film could contribute to yield a mean trap density lower than the expected trap density in the

alloy.

A further factor in the case of MP35N is the value of D_L used for the "pure" quaternary alloy. As noted above, D_L for the 50 at.% Co-50 at.% Ni alloy may well differ appreciably from the true D_L for a Co-Ni-Cr-Mo alloy. The diffusivity for 46 at.% Cu-54 at.% Ni[23] is 1.8×10^{-10} cm^2 s^{-1}, so the change from Cu to Co decreases D_L by a factor of 2, and larger decreases are likely with the addition of Cr and Mo. For example, the addition of 20 at.% Cr to Fe at 27°C decreases D_L by three orders of magnitude[5] although the effect is likely to be more pronounced for the bcc lattice of iron than for a close-packed lattice. Thus, it is quite possible that the true D_L for the quaternary alloy is somewhat lower than the D_L for the Co-Ni alloy; if so, a higher value of N_i would result. In view of the effects of the segregated sulfur and phosphorus and of a surface film, and the lack of appropriate diffusivity data for the quaternary alloy, it is still likely that the sulfur and phosphorus impurities are the principal irreversible traps in MP35N.

Comparison of Ingress Parameters

The flux of hydrogen entering the metal is somewhat higher for 4340 steel than the Monel and MP35N, largely because of the presence of an oxide film on the two nickel-based alloys. Moreover, the value of k is higher for 4340 steel, even when the rate constant approximation for MP35N is taken into consideration.

On the basis of the values of k, the principal irreversible traps appear to be MnS inclusions in the steel and, with some uncertainty, sulfur and phosphorus in the Ni-containing alloys. Because the traps in the steel are considerably larger than those in the other two alloys, they should allow a greater number of hydrogen atoms to bind per unit site, and thereby produce a higher specific saturability.

A trap with both a high binding energy and a large specific saturability for hydrogen atoms is thought to be most conducive to hydrogen

embrittlement.[10,22] In contrast, metals containing a high density of well-distributed traps with a high binding energy but a small specific saturability for hydrogen atoms should exhibit little susceptibility to interfacial cracking. Thus, the principal irreversible traps determined from the trapping constants for 4340 steel and the nickel-containing alloys are associated with markedly different susceptibilities to hydrogen embrittlement. The difference in the traps and the lower interfacial flux for the Monel and MP35N are probably key reasons these two alloys are more resistant than 4340 steel to hydrogen embrittlement.

CONCLUSIONS

The diffusion/trapping model for hydrogen ingress was shown to be applicable to the steel and nickel-based alloys provided that the alloy surface remains essentially unchanged. On the basis of this model, hydrogen ingress in these alloys was found to exhibit the following characteristics under the test conditions:

- The rate of ingress is controlled by the flux across the interface and not by hydrogen diffusion in the alloy.
- The rate constant for the flux into 4340 steel is determined primarily by electrochemical characteristics and not by alloy microstructure.
- Only about 2-3% of hydrogen atoms formed during charging enter 4340 steel and Monel K500 compared with 20-30% for MP35N.
- The proportion of hydrogen being trapped increases with the amount of hydrogen entering the alloy.
- The irreversible trapping constant and the interfacial flux of hydrogen entering the alloy are higher for 4340 steel than Monel K500 and MP35N.

The principal irreversible traps identified on the basis of the irreversible trapping constants appear to be MnS inclusions for 4340 steel and, with some uncertainty, sulfur and phosphorus clusters at grain boundaries in the Ni-containing alloys. The difference in both the nature of the traps and the interfacial flux are thought to contribute to the difference in susceptibility of 4340 steel and the two nickel-containing alloys to hydrogen embrittlement.

REFERENCES

1. E. Taylor, "Ultra High Strength Corrosion-Immune Bolting Alloys," in Proc. 1974 Triservice Corrosion of Military Equipment Conf., Vol. 1, p. 411, Wright-Patterson AFB, Ohio (1974).

2. K. D. Efird, Materials Performance **24**, 37 (1985).

3. R. McKibbin, D. A. Harrington, B. G. Pound, R. M. Sharp, and G. A. Wright, Acta Metall. **35**, 253 (1987).

4. B. G. Pound, R. M. Sharp, and G. A. Wright, Acta Metall. **35**, 263 (1987).

5. J. O'M. Bockris, M. A. Genshaw, and M. Fullenwider, Electrochim. Acta **15**, 47 (1970).

6. M. Iino, Acta Metall. **30**, 367 (1982).

7. R. A. Oriani, Acta Metall. **18**, 147 (1970).

8. A. McNabb and P. K. Foster, Trans. Met. Soc. AIME **227**, 618 (1963).

9. P. M. Driver, G. K. Campbell, R. M. Sharp, and G. A. Wright, "Hydrogen Ingress, Diffusion, and Trapping in Steel Membranes," University of Auckland, Report No. *M3/82/4 to Shell, BP, and Todd Oil Services*, New Plymouth, New Zealand (1983).

10. R. Gibala and D. S. DeMiglio, in Proc. 3rd Int. Conf. on Effect of Hydrogen on Behavior of Materials, I. M. Bernstein and A. W. Thompson, Eds., The Metallurgical Soc. of AIME, Moran, Wyoming (1980), p.113.

11. W. D. Wilson and S. C. Keeton, in Advanced Techniques for Characterizing Hydrogen in Metals, N. F. Fiore and B. J. Berkowitz, Eds., Proc. Symp. AIME, Kentucky (1981), p.3.

12. T. Asaoka, in Proc. JIMIS-2 on Hydrogen in Metals, Minakami, Jpn. Inst. Metall. (1980), p. 161.

13. J. Chene, J. O. Garcia, J. de Oliveira, M. Aucouturier, and P. Lacombe, J. Mic. Spect. Elect. **4**, 37 (1979).

14. G. M. Pressouyre, Metall. Trans. **10A**, 1571 (1979).

15. J. Y. Lee, J. L. Lee, and W. Y. Choo, in Proc. 1st Int. Conf. on Current Solutions to Hydrogen Problems in Steels, C. G. Interrante and G. M. Pressouyre, Eds., ASM, Washington, DC, p.423 (1982).

16. D. A. Shockey, D. R. Curran, and L. Seaman, "Development of Improved Dynamic Failure Models," SRI International, Final Report to U.S. Army Research Office, Contract No. DAAG-29-81-K-0123 (1985).

17. S. Trasatti, J. Electroanal. Chem. **39**, 163 (1972).

18. N. Pentland, J. O'M. Bockris, and E. Sheldon, J. Electrochem. Soc. **104**, 182 (1957).

19. J. A. Kargol and L. D. Paul, in Proc. 1st Int. Conf. on Current Solutions to Hydrogen Problems in Steels, C. G. Interrante and G. M. Pressouyre, Eds., ASM, Washington, DC, p.91 (1982).

20. R. A. Oriani, Acta Metall. **18**, 147 (1970).

21. A. J. Kumnick and H. H. Johnson, Metall. Trans. **5**, 1199 (1974).

22. G. M. Pressouyre and I. M. Bernstein, Metall. Trans. A, **9A**, 1571 (1978); Acta Metall. **27**, 89 (1979).

23. H. Hagi, Trans. Jpn. Inst. Metals **27**, 233 (1986).

24. J. A. Harris, R. C. Scarberry, and C. D. Stephens, Corrosion **28**, 57 (1972).

25. J. D. Frandsen and H. L. Marcus, "Crack Growth and Fracture in Gaseous Hydrogen", in Effect of Hydrogen in Behavior of Materials, A. W. Thompson and I. M. Bernstein, Eds., TMS-AIME, p.233 (1976).

26. D. H. Lassila and H. K. Birnbaum, Acta Metall. **35**, 1815 (1987).

27. N. Sato and K. Kudo, Electrochim. Acta **19**, 461 (1974).

28. B. MacDougall and M. Cohen, J. Electrochem. Soc. **121**, 1152 (1974); **123**, 191 (1976).

29. T. Ohtsuka, K. Schroner, and K. E. Heusler, J. Electroanal. Chem. **93**, 171 (1978).

30. R. D. Kane and B. J. Berkowitz, Corrosion **36**, 29 (1980).

Appendix A

THE BASIC PROGRAM PDP 173/488

```
REM             PAR 173/488 is to apply the potentiostatic double pulse technique
REM             using the PAR 173 Potentiostat with 276 Interface module
REM                         Address of 173/276 = 14
REM                         Terminator = CR LF ( & EOI)
REM
PRINT "Set operating mode of Model 173 to potentiostat"

OPEN "COM1:9600,N,8,2" AS 1                 :'Open communications port
PRINT #1,"REMOTE 14"                        : 'Set potentiostat to  REMOTE  with address 14

DATA -2
READ IC                                     :'Set current range code: 10 mA = -2
PRINT #1,"OUTPUT 14; I/E "IC

DATA 1
READ CG                                     :'Sets current measurement gain
PRINT #1,"OUTPUT 14; IGAIN "CG
DM=10^(-IC)*CG

DATA 0.01
READ OS                                     :'Read offset from Ecorr

PRINT #1,"OUTPUT 14; MM 2"                  :'Set modulation mode as arbitrary waveform

INPUT "|ΔE| (mV) ";EE                       :'Input magnitude of cathodic potential step
EE=-EE/1000
ED=ABS(EE)

IF ED<.02 OR ED=.02 THEN RR=0: CR=2.5       :'Set modulation range
IF ED>.02 AND ED<.2 THEN RR=1: CR=25
IF ED=.2 THEN RR=1: CR=25
IF ED>.2 THEN RR=2: CR=250
PRINT #1,"OUTPUT 14; MR "RR
EC=EE*10^6/CR                               :'EC = voltage in counts based on CR V/count


DIM II$(2000), II(2000), EC(2000)
PRINT "tc (s)","Eoc (V)","          State"
DATA 0.5, 1, 2, 5, 10, 15, 20, 25, 30, 40   :'Input charging times
FOR I=1 TO 10
READ TC(I)
PRINT TC(I),;
```

```
IF TC(I)=.5 THEN TA=1: TB=5000                    :'Set time of anodic transient and time base for sampling
IF TC(I)=1 THEN TA=2: TB=5000
IF TC(I)=2 THEN TA=2: TB=5000
IF TC(I)=5 THEN TA=5: TB=10000
IF TC(I)=10 THEN TA=10: TB=20000
IF TC(I)=15 THEN TA=15: TB=30000
IF TC(I)=20 THEN TA=20: TB=40000!
IF TC(I)>20 THEN TA=TC(I): TB=50000!

N=TC(I)*1000000!/TB                               :'Calculate number of cathodic points and anodic points
M=TA*1000000!/TB
NM=N+M

PRINT #1,"OUTPUT 14; CELL 0"                      :'Switch cell off
PRINT #1,"OUTPUT 14; READE "                      :'Read average open-circuit potential
PRINT#1,"ENTER 14"
LINE INPUT #1,E$
EOC=(VAL(E$)/1000)
PRINT EOC,;
EA=(EOC-OS)*1000
PRINT "Commenced",;

PRINT #1,"OUTPUT 14; CELL 1"                      :'Switch cell on
PRINT #1,"OUTPUT 14; SETE "EA                     :'Set potential EA

PRINT #1,"OUTPUT 14; SCV 0"                       :'Specify source curve as 0
PRINT #1,"OUTPUT 14; DCV 2"                       :'Specify destination curve as 2
PRINT #1,"OUTPUT 14; PCV 2"                       :'Specify processing curve as  destination curve (2)

PRINT #1,"OUTPUT 14; CLEAR"                       :'Clear all active points of  all curves

FOR K=1 TO N
EC(K)=EC
NEXT
FOR K=N+1 TO NM
EC(K)=0
NEXT
PRINT #1,"OUTPUT 14; LC 0,"NM                     :'Load waveform data into Processing Curve
FOR K=1 TO NM
PRINT #1, "OUTPUT 14;"EC(K)
NEXT

PRINT #1,"OUTPUT 14; COPY 2,0"                    :'Copy data to source curve
PRINT #1,"OUTPUT 14; CLR"                         :'Clear Processing Curve
PRINT #1,"OUTPUT 14; S/P 1"                       :'Specify 1 sample/point
PRINT #1,"OUTPUT 14; SIE 1"                       :'Specify current to be sampled
PRINT #1,"OUTPUT 14; TMB "TB                      :'Specify sampling time
PRINT #1,"OUTPUT 14; FP 0"                        :'Set storage location of first point as 0
PRINT #1,"OUTPUT 14; LP "NM-1                     :'Set storage location of  last point as NM-1
```

```
PRINT #1,"OUTPUT 14; NC"                    :'Initialize for curve acquisition
PRINT #1,"OUTPUT 14; TC"                    :'Commence curve aquisition
PRINT #1,"OUTPUT 14; WCD"                   :'Wait until curve is done
PRINT#1, "OUTPUT 14; CELL 0"                :'Turn cell off

PRINT #1,"OUTPUT 14; DC 0,"NM               :'Dump Processing Curve
FOR K=1 TO NM
PRINT #1,"ENTER 14"
LINE INPUT #1,II$(K)
II(K)=VAL(II$(K))/DM
NEXT

NAM$ = "E" + STR$(EE) + "T" + STR$(TC(I))   :'Store data on disk
OPEN "O", #2,  NAM$
WRITE #2, N;M;NM
WRITE #2, TA;TC(I);TB
FOR K=1 TO NM
WRITE #2, II(K)
NEXT
CLOSE #2
PRINT "Executed"
BEEP
NEXT
BEEP:BEEP:BEEP
END
```

Appendix B

THE BASIC PROGRAM INTERFACE

```
REM                INTERFACE calculates the anodic charge from the current/time transient
REM                and derives the best-fit trapping constant and flux
REM                for hydrogen ingress under interface control.
REM
REM
REM        ERF approximation constants
DATA 0.3275911, 0.254829592, -0.284496736, 1.421413741, -1.453152027, 1.061405429
READ P, A1, A2, A3, A4, A5
DATA 3.1415927, 96487
READ PI, F
DIM  K(50), R(50), SD(50), QA(40), II(1600), IA(1600)

PRINT SPACE$(50) "SELECT MODE"
PRINT SPACE$(35) "Calculate QA and QC for I/t transient ..... Q"
PRINT SPACE$(35) "Derive best-fit trapping constant ..... K"
INPUT "Mode  ";MD$

CYCLE:    INPUT "No of tc values (6) ";NC
IF NC=0 THEN NC=6
IF NC<>6 AND NC>0 THEN GOTO CHARTIME
DATA 10,15,20,25,30,40
FOR J=1 TO 6
READ TC(J)
NEXT
GOTO MODE
CHARTIME:    PRINT: PRINT "tc (s) :"
FOR J=1 TO NC
INPUT "      ";TC(J)
NEXT
MODE:    IF MD$="K" THEN GOTO RATE

REM        Integration of Current Transient
REM
INPUT "File Number ";FF
INPUT "Potential (V) ";EC
PRINT "Code for electrode area (sq. cm) :   (1)..... 4340 Steel AR  (1.267)"
PRINT SPACE$(41) "(2) ..... 4340 Steel HRc 41/54 (1.113)"
PRINT SPACE$(41) "(3) ..... MP35N (1.430)"
PRINT SPACE$(41) "(4) ..... Monel K500 AR/HRc 35 (1.267)"
PRINT SPACE$(41);:INPUT" ";AR
IF AR = 1 OR AR =4 THEN AR = 1.267
IF AR =2 THEN AR = 1.113
IF AR =3 THEN AR = 1.43
```

```
PRINT: PRINT "Input current offset for each tc:"
FOR J=1 TO NC
PRINT SPACE$(30) TC(J),;: INPUT""; IC(J)
NEXT

FOR L=1 TO NC
NAM$="E"+STR$(EC)+"T"+STR$(TC(L)) + STR$(FF)
OPEN "I",1,NAM$
INPUT #1, N, M, NM
INPUT #1, TA, TC, TB
FOR K=1 TO N
INPUT #1,II(K)
II(K)=-II(K)/AR
NEXT
FOR K=N+1 TO NM
INPUT #1,II(K)
II(K)=(-II(K)-IC(L))/AR
NEXT
CLOSE #1

REM         Calculate cathodic charge
QC=0
FOR K=1 TO N
QC=QC+(II(K)*TB*.000001)
NEXT
QC(L)=QC

REM         Calculate anodic charge
QP=0
FOR K=N+1 TO NM
QP = QP+II(K)*TB*.000001
NEXT
QP(L)=QP
NEXT

PRINT:PRINT "tc (s)" SPC(8) "Qc (mC/cm^2)" SPC(5) "Qa (mC/cm^2)"
FOR L=1 TO NC
PRINT TC(L),
PRINT USING "###.##";QC(L),:PRINT SPC(10);
PRINT USING "#.###";QP(L)
NEXT
BEEP:BEEP:BEEP

INPUT "If charge analysis is required, enter A"; CY$
IF CY$ = "A" THEN GOTO BEGIN
END
```

```
RATE:   REM         Analysis of Charge Data
REM
IF K(1)<>0 THEN GOTO BEGIN
PRINT: PRINT "Input anodic charge (mC/sq. cm):"
PRINT SPACE$(28) "tc (s)", "Qa  "
FOR J=1 TO NC
PRINT SPACE$(28) TC(J),;: INPUT "";QA(TC(J))
NEXT

BEGIN:  REM     Determine trapping constant for minimum mean deviation of flux
REM                             Initial trapping constant = 0.001 s^-1
K(1)=.001
I=1
SD(0)=100
TEST1: IF CINT(K(I))=1 OR CINT(K(I))=10 THEN GOTO PASS ELSE GOSUB CHARG
IF SD(I)< SD(I-1) OR SD(I)=SD(I-1) THEN K(I+1)=K(I)*10: I=I+1: GOTO TEST1
PASS:  KK=K(I-1)
MT=2
TEST2: K(I)=KK*MT
GOSUB CHARG
IF SD(I)<SD(I-1) OR SD(I)=SD(I-1) THEN MT=MT+1: I=I+1: GOTO TEST2
NT=1
KK=K(I-1)
TEST3:  K(I)=KK+.1*NT*KK/(MT-1)
GOSUB CHARG
IF SD(I)<SD(I-1) OR SD(I)=SD(I-1) THEN NT=NT+1: I=I+1: GOTO TEST3
NT=1
KK=K(I-1)
TEST4: K(I)=KK-.1*NT*KK/(MT-1)
IF K(I)> 0 THEN GOSUB CHARG ELSE PRINT:PRINT:PRINT"k < .0001": GOTO FINAL
IF K(I)>.0001 THEN IF SD(I)<SD(I-1) OR SD(I)=SD(I-1) THEN NT=NT+1: I=I+1: GOTO TEST4
FINAL:  K(I)=K(I-1)
GOSUB CHARG


PRINT :PRINT : PRINT  SPC(13) "_____"
PRINT:PRINT SPC(15) "tc (s)      Flux (nmol/cm^2 s)"
PRINT SPC(13) "_____"
FOR J=1 TO NC
PRINT SPC(15) TC(J),;
PRINT USING " ##.##";JJ(J)
NEXT
PRINT:PRINT SPC(15) "Rate constant = ";
PRINT USING "#.####"; K(I)
PRINT SPC(15) "Mean flux = ";: PRINT USING "##.##";MV
PRINT SPC(15) "Mean deviation = "SD(I):PRINT:PRINT
INPUT "If refinement of rate constant is required, enter R  ";RC$
IF RC$ = "R" THEN GOTO CYCLE
END
```

```
ERF:   REM        Calculate ERF Functions
REM
T=1/(1+P*Z)
Q=A2+T*(A3+T*(A4+T*A5))
E=1-EXP(-Z*Z)*T*(A1+T*Q)
RETURN

CHARG:   REM        Calculate Non-Dimensional Theoretical Charge and Flux
REM
FOR L=1 TO NC
R=K(I)*TC(L)
Z=SQR(R)
GOSUB ERF
Q1=(1-(.5/R))*E
Q2=EXP(-R)/(SQR(PI*R))
QQ=Z*(1-Q1-Q2)
JJ(L)=QA(TC(L))/(SQR(TC(L)/K(I))*F*QQ)
JJ(L)=JJ(L)*1000000!
NEXT

REM        Calculate Mean Deviation
S=0
FOR K=1 TO NC
S=S+JJ(K)
NEXT
MV=S/NC
SS=0
FOR K=1 TO NC
SS=SS+ABS(JJ(K)-MV)
NEXT
SD(I)=.0001*INT(SS*10000!/NC)
RETURN
```

END

DATE

FILMED

8-88

DTIC